DANMARKS OG GRØNLANDS GEOLOGISKE UNDERSØGELSE RAPPORT 2007/79

Mineralogical and geochemical investigations of gold-bearing Mesoarchaean supracrustal rocks from the Qussuk area, southern West Greenland

Mineral resource assessment of the Archaean Craton (66° to 63°30'N) SW Greenland Contribution no. 6

Britt Andreasen

(1 CD included)

GEOLOGICAL SURVEY OF DENMARK AND GREENLAND
MINISTRY OF CLIMATE AND ENERGY

GEUS

DANMARKS OG GRØNLANDS GEOLOGISKE UNDERSØGELSE RAPPORT 2007/79

Mineralogical and geochemical investigations of gold-bearing Mesoarchaean supracrustal rocks from the Qussuk area, southern West Greenland

Mineral resource assessment of the Archaean Craton (66° to 63°30'N) SW Greenland Contribution no. 6

Britt Andreasen

(1 CD included)

GEOLOGICAL SURVEY OF DENMARK AND GREENLAND
MINISTRY OF CLIMATE AND ENERGY

GEUS

Contents

Appendices are on the enclosed CD-ROM

APPENDICES

All supplemental appendices appear in digital format on the CD-ROM placed inside the back cover. The following list indicates the names of the digital files.

APPENDIX A – PETROGRAPHIC STUDIES

- Sample description + localities + UTM coordinates for all collected samples (87 hand specimens)
- Detailed lithological description of samples 497603 through to 497614 and samples 497685 through to 497689
- Central Qussuk peninsula (samples 497603-497614) – Hand specimen photographs & full thin section scans
- North-western Qussuk peninsula (samples 497685-497689) - Hand specimen photographs & full thin section scans

APPENDIX B – X-RAY DIFFRACTION ANALYSIS

- Central Qussuk peninsula – XRPD and Rietveld refinement files
- North-western Qussuk peninsula - XRPD and Rietveld refinement files

APPENDIX C – ELECTRON MICROPROBE ANALYSIS

- Raw data
- Measured weight percentages of oxide molecules
- Microprobe analysis results, microphotographs and backscatter images
- Calculation Table of End-member Percentages of Individual Garnet Grains
- Recalculation Scheme of Garnet Analysis into End-member Molecules – an Example

APPENDIX D – GEOCHEMICAL ANALYSIS

- ICP-MS Analysis Results, GEUS
- Chondrite normalized REE values
- ICP-OES Analysis Results, Actlabs Group of Companies
- Table displaying data for selected major and trace elements including REE detected in the samples

1. ABSTRACT

The Qussuk area is located in the eastern part of the Akia terrane, one of six terranes recognized in the Godthåbsfjord region of West Greenland. The Qussuk area represents a relict island arc complex, comprising Mesoarchaean supracrustal rocks that form a sequence of NNE-trending, isoclinally folded and steeply dipping units with a thickness of up to more than one kilometre. The supracrustal sequence has been intruded by several young components of orthogneiss and granite including the 2982 ± 7 Ma Taserssuaq tonalite complex and the 2975 ± 5 Ma Qussuk granite. Most of the Qussuk area has been metamorphosed to amphibolite facies during metamorphism in the period c. 3000-2940 Ma. The supracrustal rocks in the north-western part of the area have undergone granulite facies metamorphism and the rocks show various degrees of retrograde metamorphism to amphibolite facies. Granulite facies conditions reported from the western part of the Akia terrane were reached c. 3000 Ma.

The supracrustal rocks from the central part of the Qussuk peninsula are mainly mafic to leucocratic amphibolites characterized as greenstones and displaying mineral assemblages of quartz+plagioclase+hornblende+biotite garnet sulphides oxides. The rocks show geochemical signatures of low-K tholeiites and basalts to andesites. The supracrustal rocks from the north-western part of the Qussuk peninsula contain significant amounts of both pyroxene and amphiboles. An orthoamphibole-cordierite gneiss different from the other rocks implies an association with a massive Fe-Cu-Zn-Pb sulphide deposit. Most of the rocks presented here are collected in sulphide-mineralized layers which show extensive weathering in the form of a so-called gossan, an encrusted mass enriched in supergene minerals, in particular goethite.

Anomalous gold concentrations up to 8 ppm occur in quartz veins associated with the sulphide-mineralized amphibolites. The rocks show a significant Au-Cu association with gold as the main commodity. The dominating sulphides are pyrrhotite and chalcopyrite with significant amounts of pyrite in the auriferous rocks. Other sulphides present are sphalerite and minor pentlandite. The oxides are both primary and secondary ilmenite and magnetite and minor hematite.

Although it is difficult to settle for an origin of the gold mineralisation based on the data presented here, it is suggested that the gold formed syngenetically with the volcanic island arc either as an epithermal gold deposit or as a volcanic-associated massive sulphide gold deposit. The gold was then remobilized and deposited in quartz veins formed in fissures and fractures during deformation and/or metamorphism of the area. The original features of the ore deposit have presumably changed during the deformation and the moderate to high grade metamorphism of the area, hence impeding the origin of the gold deposit.

2. INTRODUCTION

2.1 Mineral exploration in Greenland

Natural resource extraction is a central part of the Greenlandic Home Rule's vision in the hope of creating a better economic situation in the future. It wants to turn minerals into a source of income on the same level as tourism and fishing.
Exploration for natural resources began in Greenland when the Danish-Norwegian priest Hans Egede came to the country in the beginning of the 18th century to be a missionary. Besides his missionary work he was also send there to find natural resources, and soon after his arrival the discovery of graphite occurrences was reported. More than 20 different mining operations are known from the last 150 years with the first mine opening in 1854 continuing until 1987 mining cryolite at Ivittuut. From 1990 to 2004 no mines were operating in Greenland, but recent changes (in 1991) to the Mineral Resources Act have increased interest from established mining companies around the world, and the interest for mineral prospecting in Greenland is at present the highest ever in the Greenlandic history. An example is the official opening of the Nalunaq gold mine in August 2004 which made Greenland a gold producing country. In recent years, Nunaminerals A/S has explored for mineral resources in large parts of Greenland, in particular in the Godthåbsfjord region where gold mineralization has been found on Storø. During field campaigns from 2004–2005 gold was found by GEUS in the Qussuk area for the first time.

One of the reasons why Nunaminerals A/S is one of the successful exploration companies operating in Greenland is because of today's gold prices. During the last 25 years, uneconomic gold occurrences have been re-evaluated and transformed into significant gold resources and reserves, because of the peak in gold prices in the early 1980s. Prior to this time, gold ores were defined by grades of 5 to 10 ppm in underground mines, but today because of both the enhanced economic situation, the open-pit mining and the improved mineral processing procedures, ores with ≤1 ppm Au are now considered of economic grade. Hence, the biggest obstacle (or challenge, depending on the eyes looking at it) to mining ores in areas with minor Au content is the logistic point of view.

2.2 The background to this report

The Geological Survey of Denmark and Greenland (GEUS) has for several decades worked in the Nuuk region, West Greenland to map the geological terranes of the area. A great interest has been shown in areas with greenstone belts, as these variously metamorphosed and hydrothermally altered ancient volcanic rock sequences are a known phenomenon world wide from which almost all are connected with precious ore deposits.
During the field work in the summer 2004, Adam Garde, GEUS, mapped the central part of the peninsula East of the Qussuk bay, which in this report has adopted the name the 'Qussuk peninsula'. The area is dominated by regionally metamorphosed supracrustal

rocks, and Garde sampled a rock with an anomalous gold content of 1.4 ppm. The following summer the field work, providing the basis for a Master's Thesis, was carried out by the author and Gorm Thøgersen from the University of Aarhus. The key guidelines for the field work was to explore for gold ores and the main emphasis was lain on rust-altered layers of varying widths of up to 5 m and lengths of up to several hundred meters. Three samples were collected in the central Qussuk peninsula with anomalous gold occurrences. Furthermore, a one-day reconnaissance on the north-western shore of the Qussuk peninsula yielded a rock with 5.1 ppm Au content.

This report is a shorter edition of Britt Andreasen's Master's Thesis (Andreasen 2007). To find the original thesis, please contact the library at the Geological Institute, Department of Geography and Geology at the University of Copenhagen.

3. GEOLOGICAL SETTING

3.1 The central Godthåbsfjord region

The Godthåbsfjord region is part of the Archaean North Atlantic craton in southern West Greenland and eastern Labrador, Canada dominated by polyphase banded granulite-amphibolite-facies orthogneisses (Friend & Nutman 2005). The central part of the Godthåbsfjord region is called the Nuuk region, which is an amalgation of six Arhaean tectonostratigraphic terranes. Listed by age difference starting with the oldest these are the Isukasia and Færingehavn (c. 3850 to 3300 Ma), Akia (c. 3200 to 2975 Ma), Kapisillik (c. 3075 to 2960 Ma), Tasiusarsuaq (c. 3000 to 2800 Ma), and Tre Brødre (c. 2826 to 2750 Ma) terranes. The terranes are bounded by faults and/or mylonites. Figure 1 shows the subdivisions of the Nuuk region into these terranes that have amalgamated in the period c. 2950 to 2700 Ma. The region represents a deeply eroded Archaean continent-continent collision zone (McGregor et al. 1991).

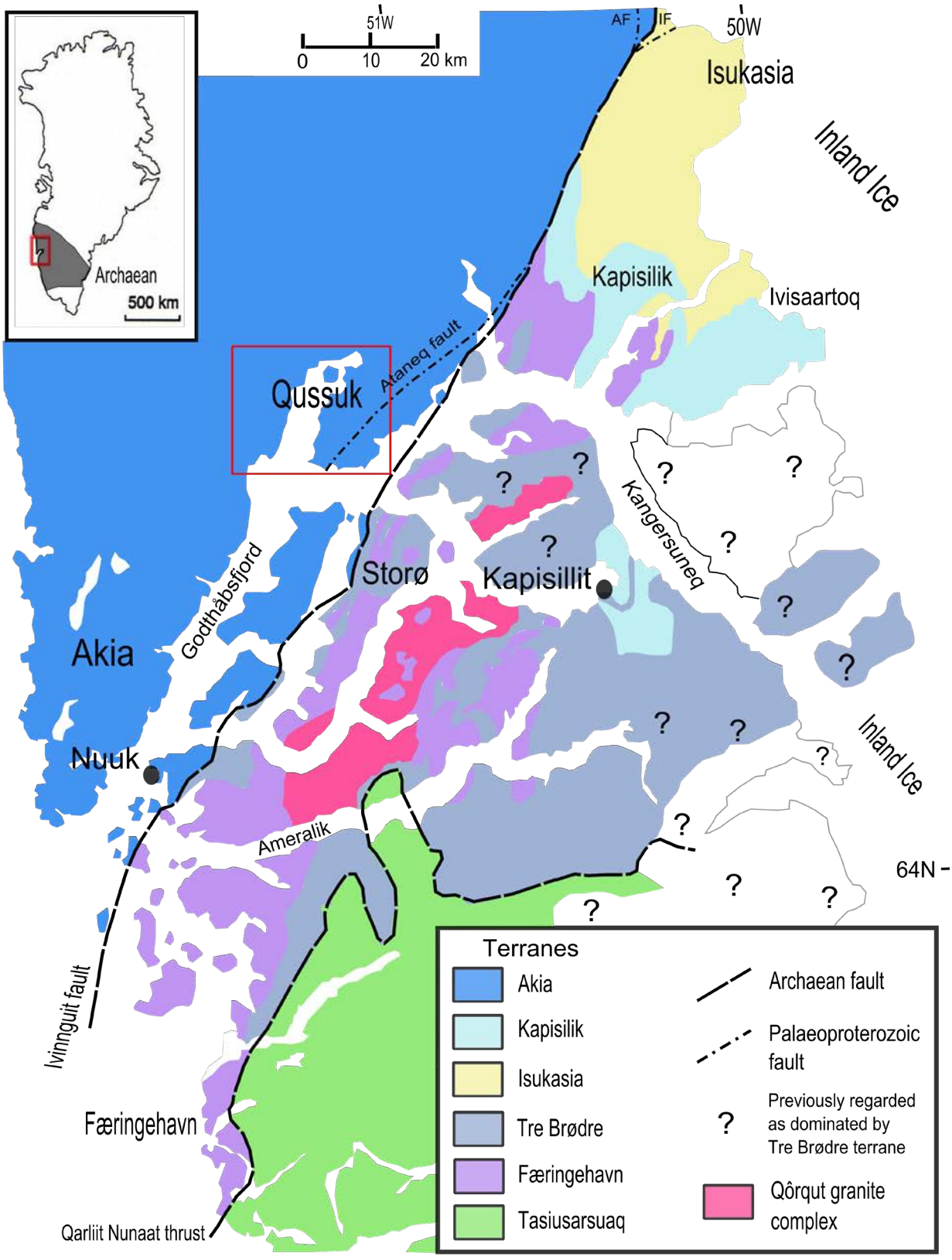

Figure 1. *A sketch map showing the distribution of the six terranes in the Godthåbsfjord region, the Qôrqut granite complex and major faults. The Qussuk peninsula studied in this thesis is marked with a red box. The previous extrapolation of the Tre Brødre terrane is now uncertain (marked with "?"). The map is modified after the map published in Friend & Nutman 2005.*

The Isukasia and Færingehavn terranes comprise similar rocks that underwent granulite facies metamorphism in many areas at c. 3600 Ma and are believed to be now dismembered parts of the same Early Archaean crust, rifted sometime in the middle Archaean. The tectonostratigraphic sequence demonstrates that the Isukasia terrane lies structurally below the Kapisillik terrane which lies below the Færingehavn terrane. This, as well as a metamorphic event c. 2950 Ma seen in the Isukasia terrane and the Kapisillik terrane, indicates that the Færingehavn and Isukasia terranes were separate units, and that the Isukasia and Kapisillik terranes had amalgamated by c. 2950 Ma. The Kapisillik and Akia terranes may also represent dismembered parts of a single middle Archaean terrane because of the fact that these two terranes comprise rocks that are similar in age and composition. The Færingehavn and the Tre Brødre terranes were formerly known as parts of the Akulleq terrane, but is now known as two terranes of different ages amalgamated ~2700 Ma. For more details concerning the geological evolution in the Nuuk region see e.g. Appel et al. (2003); Friend and Nutman (2005); Hollis et al. (2004); Polat et al. (2002, 2007).

The Tasiusarsuaq terrane to the south is differentiated from the Tre Brødre terrane by the Qarliit Nunaat fault, a c. 50-70 m wide zone composed mostly of quartzofeldspathic rocks with protomylonitic and mylonitic fabrics (Crowley 2002). Cross-cutting dykes' relationship throughout the six terranes gives a minimum age for terrane amalgamation at c. 2700 Ma. This is also the age for the regional amphibolite facies metamorphism that has been noted in the Tre Brødre and Færingehavn terranes. Postdating the regional deformation and terrane amalgamation is the c. 2530 Ma sheeted Qôrqut granite complex that cuts the Færingehavn and Tre Brødre terranes on southern Storø and further east (Hollis et al. 2004).

3.2 The Akia terrane

The northernmost terrane in the Godthåbsfjord region is the Akia terrane, most of which has been mapped at 1:100 000 scale for the Qôrqut and Fiskefjord map sheets (Garde 1989). The Akia terrane comprises Nordlandet, the Fiskefjord area, Sadeløen, Bjørneøen, the Qussuk peninsula and the North-western part of Storø. The terrane is differentiated from the Tre Brødre terrane to the southeast by the Ivinnguit fault believed to be continuous for tens of kilometres. The trace of the fault lies mostly in Godthåbsfjord but it touches the North-western shore of Storø and the South-eastern shore of Bjørneøen, crosses Sadeløen and runs through Store Malene west of Kobbefjord (Figure 1). The northern boundary of the Akia terrane is not clear but the supracrustal rocks at Kangerluarssuk is thought to maybe represent the north-western edge of the terrane (Garde et al. 2000).

The Akia terrane consists of two continental crustal complexes. One is a dioritic core dated at c. 3220 Ma and covering most of Nordlandet. The other is a voluminous complex of 3.07-2.97 Ga mainly grey tonalitic orthogneiss and supracrustal rocks between Fiskefjord and Godthåbsfjord and farther north (Hollis 2005; Garde 2007a,b). The supracrustal rocks are older than the orthogneisses that intrude them and are considered to be remnants of oceanic crust presumably in a convergent plate-tectonic setting (Garde et al. 2000; 2007a,b). The orthogneisses are of tonalitic-trondhjemitic-granodioritic (TTG) affinity.

3.2.1 The Qussuk area

The Qussuk area is located in the most eastern part of the Akia terrane (Figure 2), and has been covered by mapping for the Fiskefjord map sheet at scale 1:100.000 (Garde 1989) and discussed by Garde (1997, 2007, 2007b; Hollis et al. 2004). The Qussuk peninsula is considered to represent a Middle Archaean island arc complex with rocks dominated by relict volcaniclastic textures and andesitic compositions. The arc accretion happened just prior to the emplacement of the main group of orthogneisses (Garde 2007a,b; Garde et al. 2007). The Ataneq fault (Figure 1), a brittle fault system in a four km wide zone containing one or more systems of faults and shear zones, runs through the south-eastern part of the Qussuk peninsula with a NE-SW trend (Hollis et al. 2006). The Qussuk peninsula and Qussuk bay show two main supracrustal belts that form a sequence of NNE-trending, isoclinally folded and steeply dipping units with a thickness of up to more than one kilometer (Garde et al. 1986, 2000). The Qussuk peninsula has been subjected to several young components of orthogneiss and granite including the 2982 ± 7 Ma Taserssuaq tonalite complex and the 2975 ± 5 Ma Qussuk granite (Garde et al. 2000). The supracrustal rocks in the central and north-western part of the Qussuk peninsula provide the basis for this thesis and will be described in greater detail in section 5. The two areas are marked with red boxes in Figure 2.

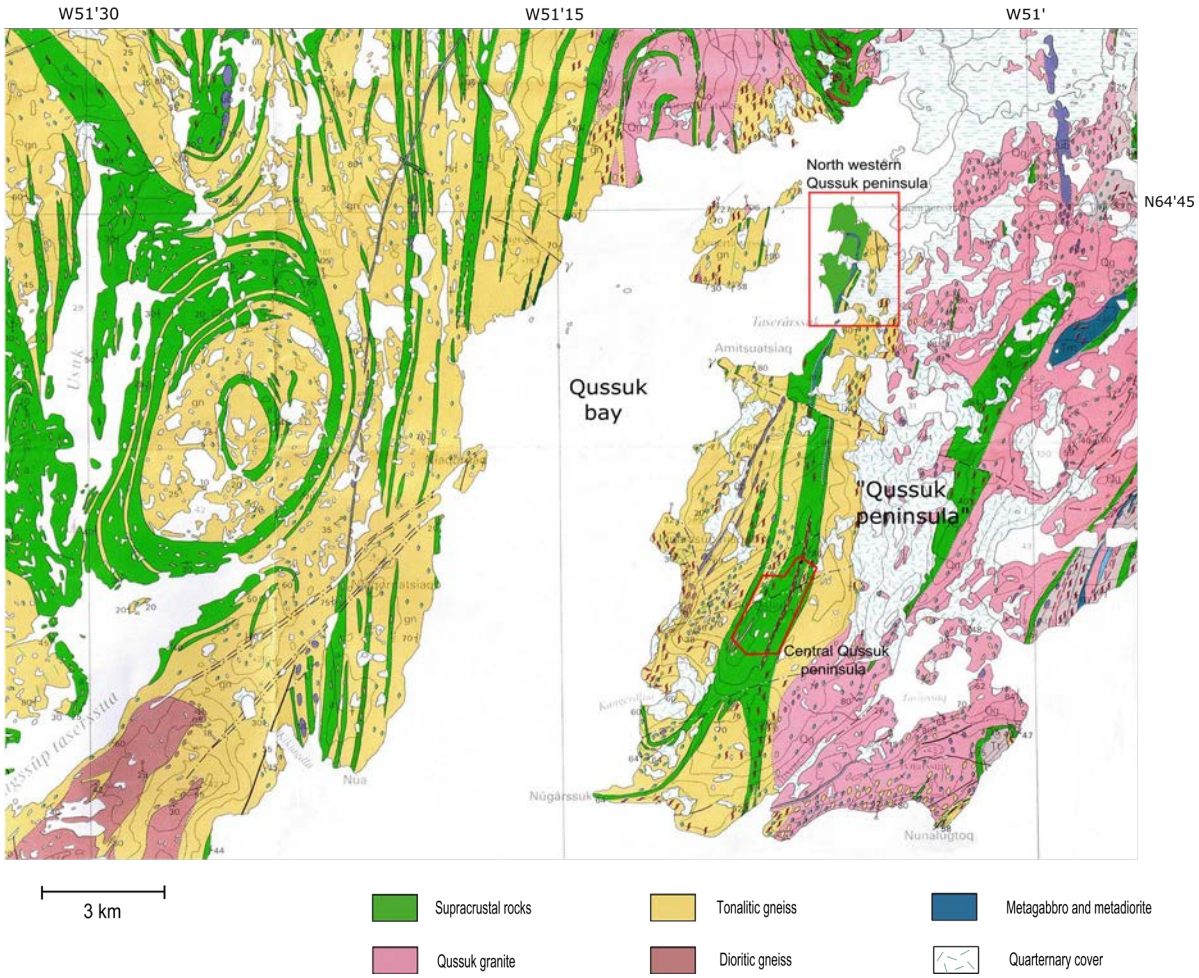

Figure 2. *The Qussuk peninsula in the eastern part of the Akia terrane (position is shown with a red box in Figure 2.1.). The two areas studied in this thesis are marked with red boxes and named the 'North western Qussuk peninsula' and the 'Central Qussuk peninsula' (Scan of the Fiskefjord map sheet 1:100 000 (Garde 1989) with modifications of the north-western Qussuk area based on map published by Garde 2007b).*

3.2.1.1 Supracrustal sequence

The supracrustal rocks consist mainly of heterogeneous banded metavolcanic amphibolites, metagabbro and ultramafic rocks (Garde 2007a,b). Leucocratic amphibolite of andesitic affinity dominates the sequence with fragmental volcaniclastic textures locally. This leucocratic amphibolite, also referred to as grey amphibolite, alternates with minor volcanosedimentary schist, minor tholeiitic amphibolite (also referred to as dark amphibolite sensu stricto) and variably altered ultramafic rocks.

3.2.2 Metamorphism of the terrane

A large part of the Akia terrane, including Nordlandet and central Fiskefjord, has been metamorphosed to granulite facies. The most south-eastern part of the terrane including the Nuuk peninsula, Sadeløen, Bjørneøen and part of the Qussuk peninsula was only metamorphosed to amphibolite facies (McGregor et al. 1991). Zircons from a fragmental

metavolcanic rock collected by Garde at the central Qussuk peninsula give an age of amphibolite facies metamorphism in the period c. 3000-2940 Ma (Hollis 2005). A large area in between these two areas has been variably retrogressed from granulite facies to amphibolite facies, and at least part of this retrogression was the result of influx of water associated with late deformation (Pâkitsoq phase, see below).
The granulite facies conditions were reached at c. 3000 Ma (Garde 1997), and they have been proposed to be the result of repeated injections of hot tonalitic magmas into the growing continental crust since it culminated during or just after emplacement of TTG gneisses in the terrane. Peak metamorphic conditions at 800 ± 50°C and 7.9 ± 1.0 kbar are found on Nordlandet (Riciputi et al. 1990).

3.2.3 Deformation of the terrane

The structural evolution of the entire Akia terrane may be represented by the structures found in various parts of the Fiskefjord area (Garde 1997). Complex multiple folded outcrop patterns, changing orientations of structural elements and structures up to 10 km in size characterize the various parts and appear to have been developed during the early phases of the c. 3000 Ma metamorphism and thereby accretion of the continental crust.
Three main phases of deformation have been recognized by Berthelsen (1960) around central Fiskefjord (the Tovqussap nunâ peninsula). The first two phases named Midterhøj and Smalledal show large recumbent isoclinal folding with first NW to NS trending and then ENE to NE trending axes. The following deformation phase, the Pâkitsoq phase which refolded the Midterhøj and Smalledal phases, resulted in a series of upright to overturned NE to N-S trending folds. This phase of deformation was simultaneous with the culmination of the granulite facies metamorphism in the area (see above). A fourth subsequent deformation phase recognized at the Tovqussap nunâ peninsula shows localized steep high strain zones developed under retrogressive amphibolite facies conditions. This phase has not been recognized anywhere else in the Akia terrane (all from Berthelsen 1960; Garde et al. 2000).

3.3 Recent exploration for gold in the central Godthåbsfjord region

Interest in the economic potential of the Nuuk region took form in the 1990s led by Nunaoil A/S, who explored for gold and base metals in the Archaean Isua greenstone belt as well as on Storø. After three years of exploration on Storø, NunaOil A/S initiated drilling for gold in 1995 at two prospecting areas named Qingaaq and Aappalaartoq (Appel et al. 2000; Knudsen et al. 2007; Juul-Pedersen et al. 2007; Nutman et al. 2007). Rio Tinto Mining and Exploration, Ltd., carried out diamond drilling for hematite ore concealed under the Inland Ice in the Isua greenstone belt in the late 1990s (Appel et al. 2000).

NunaMinerals A/S was established in 1998 with a view to taking over the mineral activities from NunaOil A/S and is the sole owner of the gold occurrence on Storø. NunaMinerals A/S is now trying to find an international collaborator to bring the project further economic and technical competence. Localities in the Nuuk region that have shown Au, Cu and PGE are

presented with red and light blue stars in Figure 3. Nunaminerals A/S prospecting in the Qussuk area in 2006 has given promising results with high gold values in sediment samples and rock samples yield up to 21.7 ppm Au ("Alle Nyheder; Meddelelse nr. 13/2006", 2007, 5 December). In 2007 four drill targets for gold and copper have been identified by geophysical investigations in the Qussuk area ("Alle Nyheder; Meddelelse nr. 35/2007", 2007, 5 December).

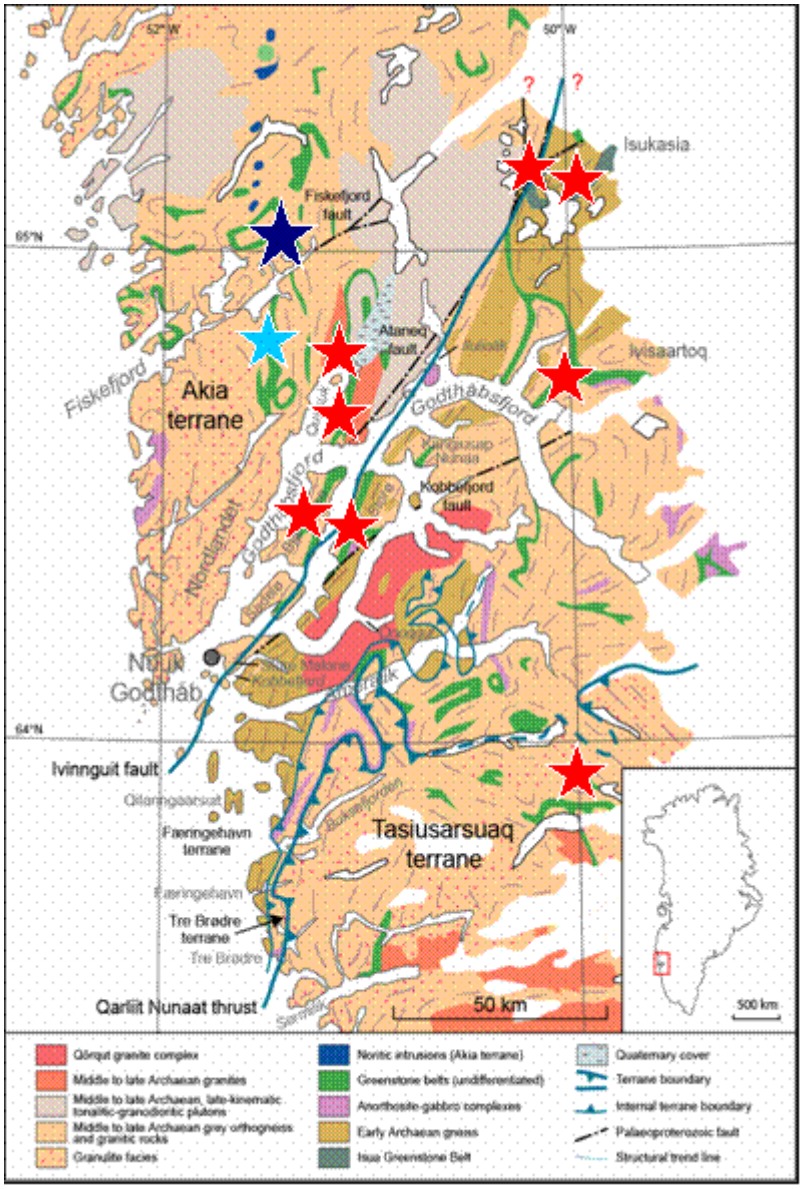

Figure 3. *Geological map of the Nuuk region modified from Escher & Pulvertaft (1995). Red stars indicate gold occurrences. Dark blue star is the Seqi olivine deposit and light blue star is Pd-Pt occurrences south of Fiskefjord*

4. MATERIALS AND METHODS

4.1 Samples

Rock samples were collected throughout the whole Qussuk area. A total of 89 samples in varying sizes from 300 grams to one kilogram were collected and given the numbers 497601 through to 497689. From the central part of the Qussuk peninsula 75 rock samples were collected during 11 effective days in the field between 19 July 2005 and 2 August 2005. Nine samples were collected from the head of the Qussuk bay and five samples were collected from the north-western part of the Qussuk peninsula during a one-day reconnaissance on 6 August 2005. At several locations the samples were collected systematically along cross sections to help the understanding of the stratigraphic column of the area.

Petrographic descriptions of all collected samples as well as bearings of the geological localities can be found in Appendix A. Out of the collected samples 17 have been considered in this report. 12 of the samples represent a profile line in the central part of the Qussuk peninsula and five of the samples represent the area in the north-western part of the Qussuk peninsula.

4.2 Petrographical and geochemical studies

A total of 17 thin sections (one normal and 16 polished) were made in the Thin Section and Sample Preparation Laboratory at GEUS. Photomicrographs of selected minerals were taken with a Zeiss Axioskop 40 Pol at GEUS. Scanned images of the full thin sections as well as photographs of the 17 hand specimens studied in this thesis can be found in Appendix A.
Electron microprobe analyses were carried out on three thin sections (samples 497605, 497609 and 497689) at the microprobe facilities at the Geological Institute, University of Copenhagen using a JEOL JXA-8200 Superprobe.
Mineral separation including the use of a CWC magnet, a Frantz Isodynamic Magnetic Separator (FIMS) as well as density separation, was conducted on 11 samples in the Separation Laboratory at the Geological Institute, University of Copenhagen, in order to get easier readable X-ray powder diffraction patterns.

X-Ray Diffraction was used to identify and characterize minerals in 13 rock samples. The result is a total of 35 X-ray powder diffraction patterns using a Phillips X-ray powder diffractometer, and unit cell parameters were found for three minerals by single crystal X-ray diffraction using a Bruker AXS four-circle X-ray diffractometer equipped with a Smart CCD detector. Both instruments are found at the X-Ray Powder Diffraction Laboratory at the Geological Institute, University of Copenhagen.
Instrumental Neutron Activation Analysis (code 1H-Au + 48) and Inductively Coupled Plasma Optical Emission Spectrometry (code 1F) applied to 63 samples were performed by the Actlabs Group of Companies (AGC), Canada. Owing to the semi-quantitative character of

the analyses performed by the AGC another trace element analysis was conducted by Jørgen Kystol, GEUS on Inductively Coupled Plasma Mass Spectrometry (PerkinElmer Elan6100DRC). A total of 16 samples were measured giving qualitative results of 36 trace elements.

5. RESULTS

5.1 The central Qussuk peninsula

5.1.1 Geological map

The central part of the Qussuk peninsula was originally mapped by Adam A. Garde (GEUS). The detailed map with a few modifications is shown in Figure 4. Bearings and associated rock samples of the localities (B.Andreasen, BAN) on the map are shown in Table 1. In the following the range of colours used on the map is shown in brackets after each lithology. The dominating lithology of the supracrustals is a banded amphibolite. The amphibolite is divided into three units; (1) a grey amphibolite covering most of the area and with bands displaying fragmental texture (light green), (2) a dark grey amphibolite sensu stricto (dark green) and (3) a black amphibolite which shows different degrees of hydrothermal alteration and varying magnetite content (blue). Several sulphide-mineralized layers in the grey amphibolite extending over hundreds of meters in length and up to 5 m in width are characteristic for the area (red). Two thin bands of metagabbro (bright green) and an ultramafic body (possibly peridotite – field term) (purple) associated with the hydrothermally altered amphibolite are observed. Intrusives of tonalitic (skin colour), granitic (light pink) and dioritic-mafic tonalitic (orange) gneisses cover large parts of the area with the tonalitic gneiss as the dominating type. The general strike/dip of the area is NNE/72-86.

Locality	Bearings	Sample no.	Rock type
BAN-01	N 64.65392 W 51.14022	497628	Hydrothermal altered extremely magnetic, black rock.
		497629	Hydrothermal altered non-magnetic black rock.
		497630	Hydrothermal altered rock zoned w. black and green layers without distinct boundaries.
		497631	Hydrothermal altered greenish rock w. quartz vein.
BAN-02	N64.65052 W51.14405	497627	Hydrothermal altered black rock w. quartz veins and nodules.
BAN-03	N64.65121 W51.13601	497623	Dark amphibolite w. sulphides, disseminated and aggregates.
		497624	Rust altered white rock w. disseminated sulphides.
		497625	Garnet amphibolite w. sulphides, disseminated and aggregates.
		497626	Dark amphibolite w. few disseminated sulphides associated w. quartz nodules.
BAN-04	N64.65793 W51.14348	497601	Pyroclastic rock.
BAN-05	N64.65787 W51.13161	497602	Dark amphibolite w. few disseminated sulphides.
BAN-07	N64.66916 W51.12238	497603	Dark amphibolite.
		497604	Grey (garnet) amphibolite.
		497605	Garnet-rich rock.
		497606	Dark amphibolite.
		497607	Garnet-mica gneiss.
BAN-08	N64.66907 W51.12122	497612	Biotite-quartz amphibolite.
		497613	Garnet amphibolite w. quartz veins.
		497614	Grey amphibolite.

BAN-09	N64.66918 W51.12272	497608	Rust altered siliceous rock w. disseminated sulphides <2 mm.
		497609	Garnet amphibolite.
		497610	Dark amphibolite w. quartz veins and disseminated sulphides.
		497611	Dark amphibolite w. quartz veins and disseminated sulphides.
BAN-10	N64.65134 W51.14298		*Eastern margin of ultramafic body.*
BAN-11	N64.65087 W51.14424		*Western margin of ultramafic body.*
BAN-12	N64.65031 W51.14543	497615	Tonalite – granitic rock rich in dark minerals.
BAN-13	N64.65056 W51.14867	497616	Dark amphibolite (sensu stricto).
BAN-14	N64.65198 W51.13517	497617	Quartz-garnet-biotite rock w. disseminated sulphides <3 mm.
		497618	Quartz-garnet-biotite rock.
		497619	Quartz and sulphide-rich rock.
		497620	Sulphide-rich rock w. quartz nodules.
		497621	Quartz-biotite gneiss w. large amount of sulphides.
BAN-15	N64.6526 W51.13396	497622	Quartz-rich rock w. disseminated sulphides.
BAN-16	N64.65201 W51.13525	497632	Black amphibolite w. white grains having a rust-coloured halo.
BAN-17	N64.65108 W51.13547	497633	Dark amphibolite.
		497634	Light grey amphibolite w. disseminated sulphides <1 mm.
		497635	Dark amphibolite w. few quartz veins and few disseminated sulphides.

		497636	Dark amphibolite w. quartz veins up to 2 cm in width and disseminated sulphides.
		497637	Dark amphibolite w. sulphides, disseminated and aggregates.
		497638	Dark amphibolite w. disseminated sulphides.
		497639	Garnet-biotite amphibolite w. disseminated sulphides.
		497640	Grey amphibolite w. disseminated sulphides.
		497641	Grey amphibolite.
BAN-18	N64.65107 W51.13648	497642	Garnet amphibolite.
		497643	Dark amphibolite w. quartz veins and sulphide aggregates.
BAN-19	N64.65357 W51.1336	497644	Rust altered grey amphibolite w. disseminated sulphides.
		497645	Dark amphibolite w. few quartz veins.
BAN-20	N64.65372 W51.13435	497646	Metagabbro.
BAN-21	N64.65395 W51.13476	497647	Dark amphibolite.
BAN-22	N64.65444 W51.13772	497648	Dark amphibolite w. few, thin quartz veins.
		497649	Metagabbro.
BAN-23	N64.65456 W51.15286	497650	Grey amphibolite w. disseminated sulphides.
		497651	Grey amphibolite w. disseminated sulphides.
		497652	Rust altered quartz-rich rock w. disseminated sulphides.
		497653	Gabbro w. green mineral veins.
BAN-24	N64.65403 W51.1518	497654	Dark grey amphibolite w. disseminated sulphides.
		497655	Dark amphibolite w. quartz veins.
		497656	Grey amphibolite.

BAN-25	N64.65532 W51.15219	**Photo**.	Pyroclastic rock.
BAN-26	N64.6577 W51.12992	497657	Quartz-biotite rock w. sulphides, disseminated and aggregates.
		497662	Dark amphibolite w. few garnets.
BAN-27	N64.66395 W51.13074		*Qussuk's highest point.*
BAN-28	N64.66367 W51.13187	497658	Quartz-rich rock w. sulphide aggregates.
BAN-29	N64.65923 W51.14375	497659	Grey amphibolite w. disseminated sulphides.
		497660	Grey amphibolite w. sulphides, disseminated and aggregates.
BAN-30	N64.65703 W51.13057	497661	Quartz- and plagioclase-rich rock w. disseminated sulphides.
BAN-31	N64.66354 W51.12368	497663	Garnet amphibolite w. quartz vein.
		497664	Rust altered grey amphibolite.
		497665	Dark amphibolite w. quartz veins.
		497666	Garnet amphibolite w. disseminated sulphides.
BAN-32	N64.66385 W51.12523	497667	Garnet amphibolite.
BAN-33	N64.66963 W51.12247	497668	Dark amphibolite w. quartz veins.
		497669	Dark amphibolite w. quartz veins.
BAN-35	N64.65017 W51.1439	497670	Hydrothermal altered green rock.
		497671	Hydrothermal altered magnetic, black rock.

BAN-36	N64.65136 W51.14301	497672	Ultramafic rock (peridotite).
BAN-37	N64.65628 W51.14711	497673	Pyroclastic rock.
		497674	Hydrothermal altered magnetic, black rock.
BAN-38	N64.65723 W51.14433	497675	Pyroclastic rock.

Table 1. *Bearings, associated rock samples and types connected to the localities (B.Andreasen, BAN) on the detailed map of the central part of the Qussuk peninsula (Figure 4).*

The modifications made to Adam A. Garde's map (Garde 2004) are as follows: A large band mapped as amphibolite sensu stricto is now mapped mainly as grey amphibolite with only a thin band of amphibolite sensu stricto next to a unit of metagabbro. An extension of a sulphide mineralized band south of the lake in the mid-west area has been observed and mapped. The area of hydrothermally altered amphibolite south of the camp was observed to be larger than it appears on the original map and additionally recognized on the southern side of the ultramafic body. The ultramafic body was observed to be smaller than originally mapped.

5.1.2 Supracrustal lithologies

Amphibolites

The banded amphibolite in different shades of grey is a lineated, fine to medium grained rock with a mineral association of quartz, plagioclase, biotite and amphibole. Several units of the grey amphibolite show a content of disseminated iron sulphides, dominated by pyrrhotite, chalcopyrite and pyrite. Additionally, garnet is present in many bands of the grey amphibolite with varying grain sizes from millimetres to centimetres. In some areas the amphibolite shows a fragmental texture of pyroclastic or volcanoclastic origin (BAN 04). The clasts show obvious different rock types (e.g. gabbro, granite, anorthosite) and shapes (Figure 5). Boudins of a green, fine grained, competent rock unit (c. 10x40 cm in size) occur in the grey amphibolite (BAN 06, Figure 6). The rock recognized as boudins is considered to be of the same altered character that is seen in the hydrothermally altered rock units in the area (see below). Hence the alteration zone is pre-dating the deformation of the area that formed the boudins (described in section 3.2.3). The boudin neck is a white, coarse grained intrusive body of granitic/pegmatitic character.

The dark amphibolite sensu stricto is a mafic, lineated, fine grained rock with medium sized crystals of amphibole. It has a mineral association of quartz, plagioclase, biotite and amphibole. It contains few disseminated sulphides, garnet porphyroblasts and small quartz aggregates.

Figure 4. *A detailed map of the central part of the Qussuk peninsula showing the different lithologies within the supracrustal sequence. All the BAN localities (B.Andreasen) as well as the AAG locality 187 (Garde 2004) are plotted. The dark blue line in the upper part of the map marks the profile shown in detail in Figure 11. Modified after A.Garde 2004.*

Figure 5. *Visible clasts of different rock types in the grey amphibolite giving the rock a fragmental texture of possibly pyroclastic origin.*

Figure 6. *Boudins c. 10 x40 cm in size of a green, fine grained rock in the grey amphibolite. The rock resembles the hydrothermally altered units hence implying that the alteration took place prior to the deformation of the area.*

The black amphibolite is a mafic, fine grained, black to greenish black rock with a mineral association of amphibole (hornblende), clinopyroxene (augite), <5% quartz and oxides (magnetite and ilmenite). The homogenous unit of the black amphibole shows varying degree of magnetism from non-magnetic to extremely magnetic. In the clast-filled unit the content varies from abundant to none of calc-silicate (possibly epidote and/or diopside) clasts of centimetre sizes. The rock is chemically weathered leaving holes with a brown halo in the matrix presumably after the calc-silicate minerals.

Other mafic rocks

The peridotite is an ultramafic, medium to coarse grained, magnetic rock with a mineral association of olivine, pyroxene, biotite and magnetite. Coarse grained pyroxene sticks out giving the rock a spotted texture.

The metagabbro is a medium grained, intermediate black and white rock. Pronounced black grains protrude on the surface giving the rock a spotted texture. The mineral assemblage is plagioclase and pyroxenes. It is recognized at two localities (BAN 20, 22) as thin bands formed as lenses being between 10-20 m wide and 50-100 m long within the grey amphibolite.

Intrusions

Intrusives of tonalitic and granitic composition cross cut the supracrustals. Most of these intrusions belong to the Taserssuaq tonalite complex and the Qussuk granite, which have been dated at c. 2975 Ma and thus provide a minimum age for the supracrustal rocks (Hollis et al. 2004). The tonalite is a light grey, homogeneous, coarse grained rock rich in biotite and hornblende and with a content of ~40% quartz and plagioclase. In Figure 7 the dark amphibolite sensu stricto is intruded by the tonalite which shows evidence that the deformation of the area has happened prior to the intrusion of the tonalites and thereby giving a minimum age of the collision of the terranes.

Figure 7. *Tonalitic intrusive in a dark amphibolite sensu stricto. The tonalite shows evidence that the deformation of the area has happened prior to the intrusions of the tonalite.*

5.1.3 Sulphide-mineralized layers

The sulphide-mineralized layers in the grey amphibolite run parallel to the general trend in the supracrustal sequence. They have varying thicknesses from tens of centimetres to metres and can be followed for up to hundreds of meters. A distinguishing rust altered red-yellow-brown colour on the surface makes them easy to identify (Figure 8). The sulphide-mineralized layers farthest towards the west of the area contain very small amounts of visible disseminated iron sulphides. The layers in the eastern and northeastern parts of the area have a high content of disseminated and aggregated iron sulphides with grain sizes up to 7 mm. Pyrrhotite, chalcopyrite and pyrite are the main sulphide content associated with covellite and sphalerite. Other secondary minerals associated with the sulphide mineralisation are oxides, mainly ilmenite and occasional magnetite. Some of the layers have a medium to high content of garnet with grain sizes up to several centimeters.
The rust alteration is due to weathering and many of the rock specimens collected from the layers are strongly rust altered throughout the rock. The mineral goethite is recognized as the alteration product of the iron-sulphides.

Figure 8. *The characteristic yellow-brown-red colour of the rust altered layers in the grey amphibolite.*

5.1.4 Hydrothermal alteration

Areas of intense hydrothermal alteration of the black amphibolite occur at several localities. The altered layers show different content of clasts from none to many and varying degree of magnetism from non-magnetic to extremely magnetic. In Figure 9 units of up to 0.5 m in width of a clast-rich rock (sample 497673) and a magnetic rock (sample 497674) alternate. This sequence at locality BAN 37 represents hydrothermally altered sequences throughout the area although the division of the alternating layers is not necessarily as distinct in other areas. The altered layer in the south-central part of the map (e.g. locality BAN 1) is most likely of ultramafic composition showing different degrees of hydrothermal alteration. There

is a possibility that the peridotite and the hydrothermally altered layer formed in the same system, e.g. hydrothermal alteration could have happened simultaneously with the emplacement of the ultramafic layer.

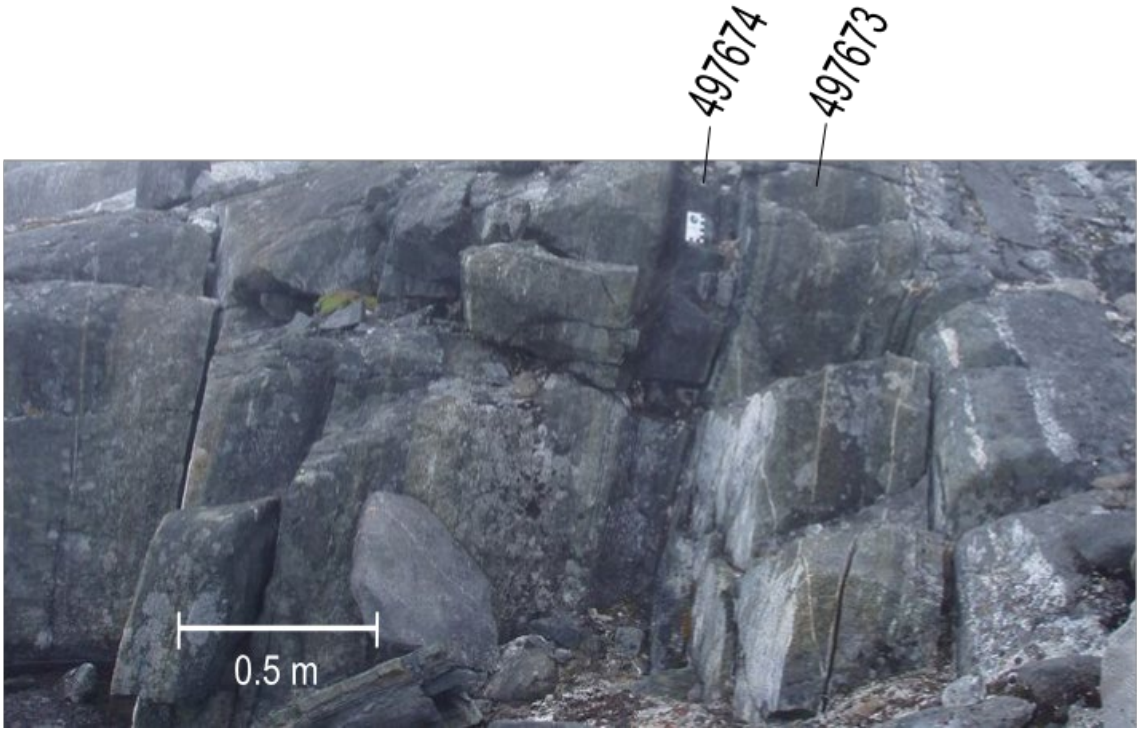

Figure 9. *Locality BAN 37. A sequence representing hydrothermally altered units of the whole area. Sample 497673 presents a green clast-filled rock. Sample 497674 presents a black magnetic rock.*

Hydrothermal alteration of one layer of the dark amphibolite *sensu stricto* is recognized as units with excessive garnet content.

5.2 Auriferous profile at central Qussuk peninsula

5.2.1 Profile line

Anomalous gold concentrations of up to 8.1 ppm have been found in the northern most part of the central Qussuk area (marked with a red box in Figure 2). Along a profile line 12 samples (497603 to 497614) were collected. Detailed mineralogical descriptions as well as photomicrographs can be found in Appendix A. From the 12 samples 11 polished thin sections, 24 XRPD patterns and 11 REE patterns have been used to describe the rock units. Thin sections and XRPD patterns are not available for samples 497603 and 497604.
The profile line (Figure 11) is c. 80 m long running NW-SE from locality BAN 08 with bearings N 64°40.144', W 51°07.273' to locality BAN 09 with bearings N 64°40.151', W 51°07.363'. Locality BAN 07 with bearings N 64°40.150', W 51°07.343' is the approximate

centre of the profile line. The profile shows NNE-trending layers consistent with the general trend in the supracrustal sequence in the area. It is located in the vicinity of Garde's locality 187 from 2004, from where a rock with 1.4 ppm Au was collected (Hollis et al. 2004).

The profile contains several rust altered layers in the grey amphibolite alternating with layers of dark amphibolite *sensu stricto* and intruded by tonalitic gneiss. Sample 497603 represents the dark amphibolite that is characteristic for the area and is considered a "sensu stricto" type. Sample 497604 is representative of grey amphibolite. Figure 10 (BAN 07) shows three bands of dark amphibolite within the grey amphibolite and framed by tonalitic intrusives. The bands of dark amphibolite are <0.5 m wide. Tonalitic intrusives also cut and run parallel with the dark amphibolite bands and confirm the younger age of the intrusives in the area.

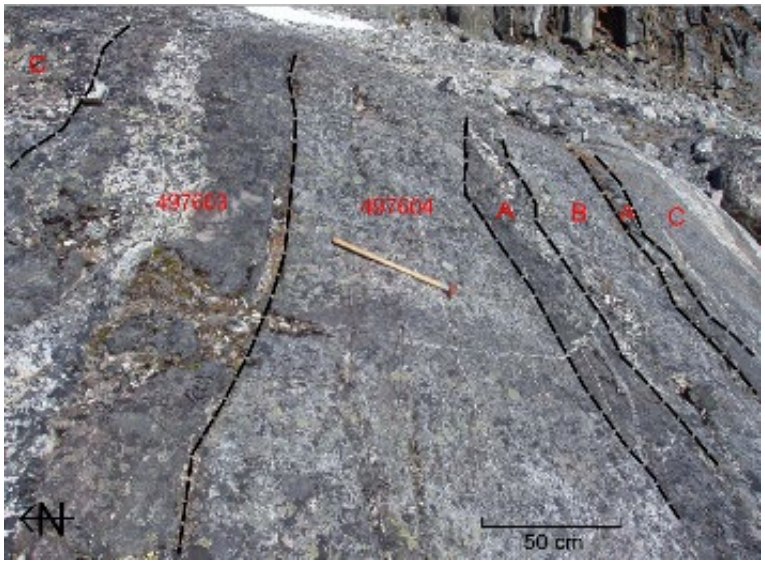

Figure 10. *Three bands of dark amphibolite (sample 497603 + areas marked A) within the grey amphibolite (sample 497604 + area marked B). The dark amphibolite bands are cut by several granitic veins running parallel to the NNE trend of the sequence. On each side (areas marked C) are bands of tonalitic intrusives.*

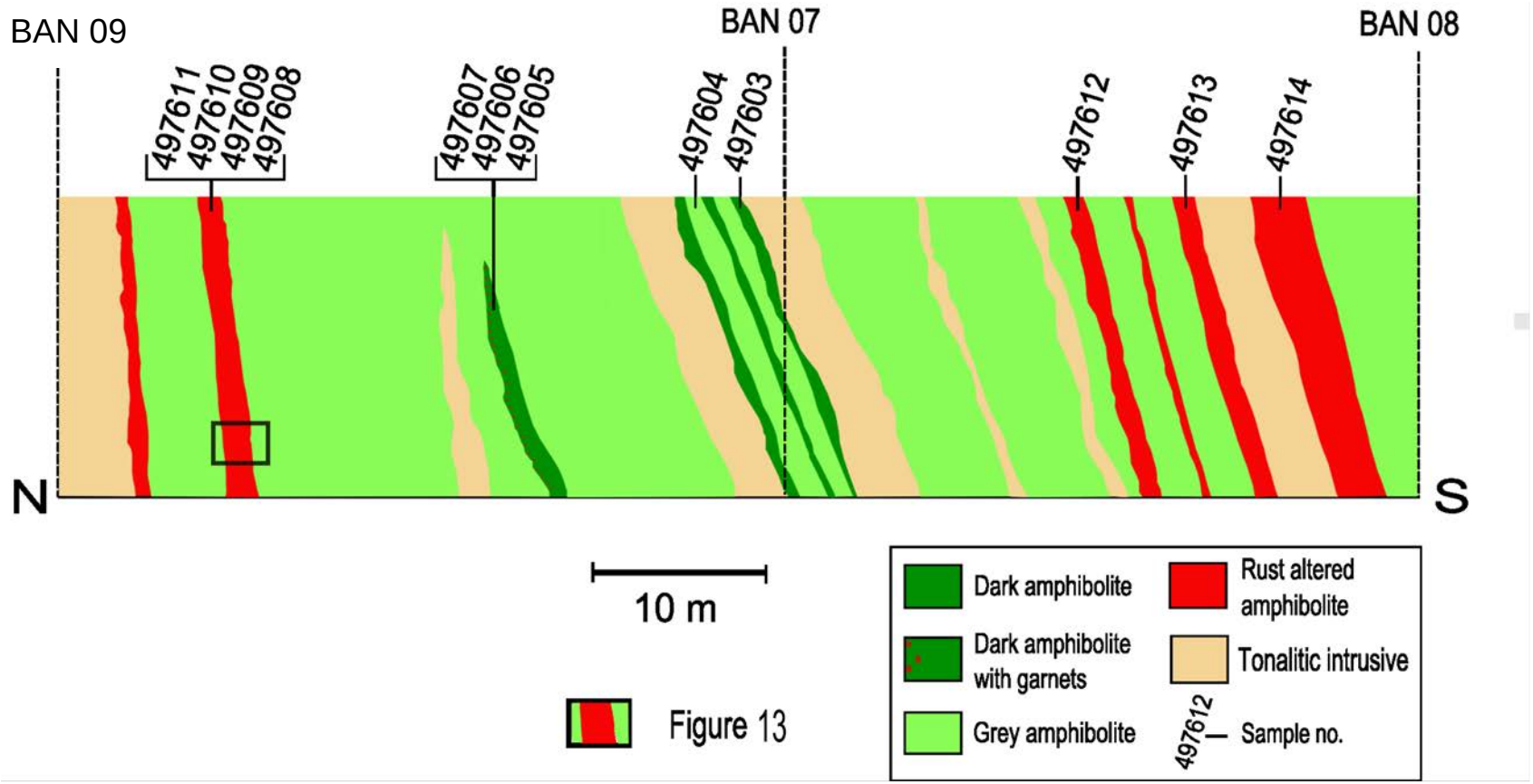

Figure 11. *The auriferous profile line from the central part of the Qussuk peninsula showing layers trending north-northeast. The sample numbers and localities are shown above the profile. The grey and dark amphibolites are in shades of green, the rust altered layers are in red and the tonalitic intrusives are in light brown. An area with excessive garnet content in a band of dark amphibolite is shown with dark red dots (see also Figure 13).*

Samples 497605, 497606 and 497607 are collected in a band of dark amphibolite *sensu stricto* which shows anomalous garnet content of up to 70%. Figure 12 shows the rock unit succession of the three samples. Two garnetiferous units represented by samples 497605 and 497607 are divided by a dark amphibolite *sensu stricto* with only a few garnet porphyroblasts and <5% disseminated pyrrhotite represented by sample 497606. In the garnetiferous unit (sample 497605) two round cores (c. 15 cm in diameter) of a fine-grained grey rock with no garnet content occur. The cores are encircled by a zone of outward increasing garnet content (Figure 12B).

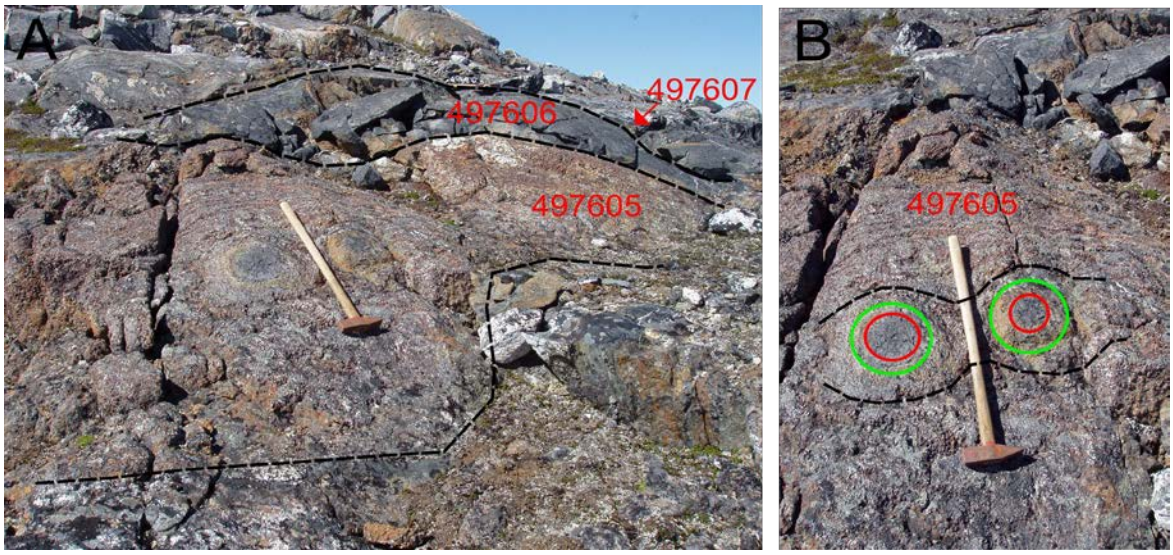

Figure 12. *Dark amphibolite sensu stricto with anomalous garnet content.* ***A****. Unit succession of sample 497605 with garnet content of up to 80% with the overlying dark amphibolite sensu stricto, sample 497606. Sample 497607, a rust altered garnetiferous rock, is not in the picture but its position is shown by the red arrow.* ***B****. A close-up of the garnet rich rock with the garnet-lacking cores (red circles) encircled by a zone of alteration (green circles) with outward increasing garnet content.*

Samples 497608, 497609, 497610 and 497611 are collected in a c. 2 m wide rust altered sulphide-mineralized, auriferous layer. Figure 4.10 shows a more detailed section of the distribution of the units within the layer. Sample 497608 represents a c. 30 cm wide siliceous unit which locally contains remnant amphibolite. The sample contains up to 10% of anhedral, fine to coarse grained pyrite and chalcopyrite plus minor pyrrhotite and covellite. The sulphides are disseminated throughout the sample but with areas of larger concentrations (Figure 14A). A few pyrite grains are observed with euhedral form but rounded edges (Figure 14B). Samples 497609 and 497611 both represent garnetiferous amphibolite units of c. 50 cm and 70 cm widths, respectively. Sample 497609 contains ~3% disseminated sulphides which are anhedral, very fine grained chalcopyrite, pyrrhotite, covellite and sphalerite. Sample 497611 contains <10 % sulphides. The sulphides are disseminated fine to medium grained chalcopyrite, pyrrhotite, marcasite and covellite. Chalcopyrite and pyrrhotite occur in the same grains. Several pyrrhotite grains are interconnected with euhedral biotite. One example is shown in Figure 14C. A sulphide and biotite rich unit ~50 cm wide represented by sample 497610 is found in between the garnetiferous units. The sample

contains up to 25% sulphides. The sulphides are disseminated anhedral fine to coarse grained chalcopyrite plus pyrrhotite, pyrite, marcasite, covellite and sphalerite. Several grains have been wholly or partly replaced by goethite showing boxwork textures (Figure 14E+F). Rounded, very fine grained sulphides with high reflectance (possibly arsenopyrite) occur as inclusions in silicate grains. Most pyrrhotite grains show an alteration zone of marcasite replacement, which formed during weathering of pyrrhotite. In some grains the very distinctive 'bird's-eye' texture is seen (Figure 14D), composed of marcasite replacing pyrrhotite (Craig and Vaughan 1994).

Samples have been collected from three rust altered layers in the south-westernmost end of the profile. Samples 497612 and 497613 which contain only minor sulphides and oxides, are collected in two c. 1.5 m wide rust altered layers divided by grey amphibolite and a c. 3 m wide rust altered layer cut by a c. 0.7 m wide pegmatite vein (BAN 08) is represented by sample 497614.

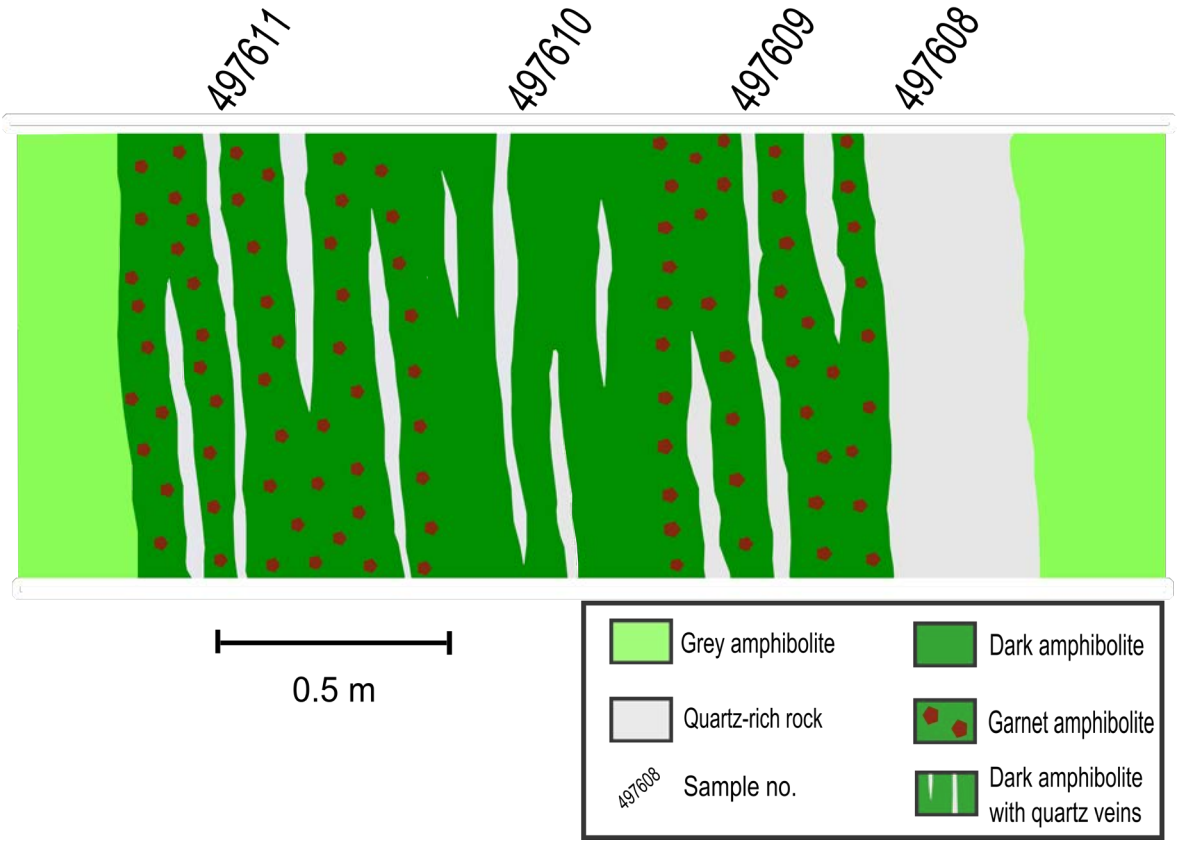

Figure 13. *A detailed section of the auriferous units' distribution in a c. 2 m wide rust altered layer in the grey amphibolite. The sample numbers are shown above the units. Amphibolites are shown in shades of green and garnetiferous amphibolite is marked with dark red pentagons. Quartz as veins and the siliceous rock unit are shown in grey.*

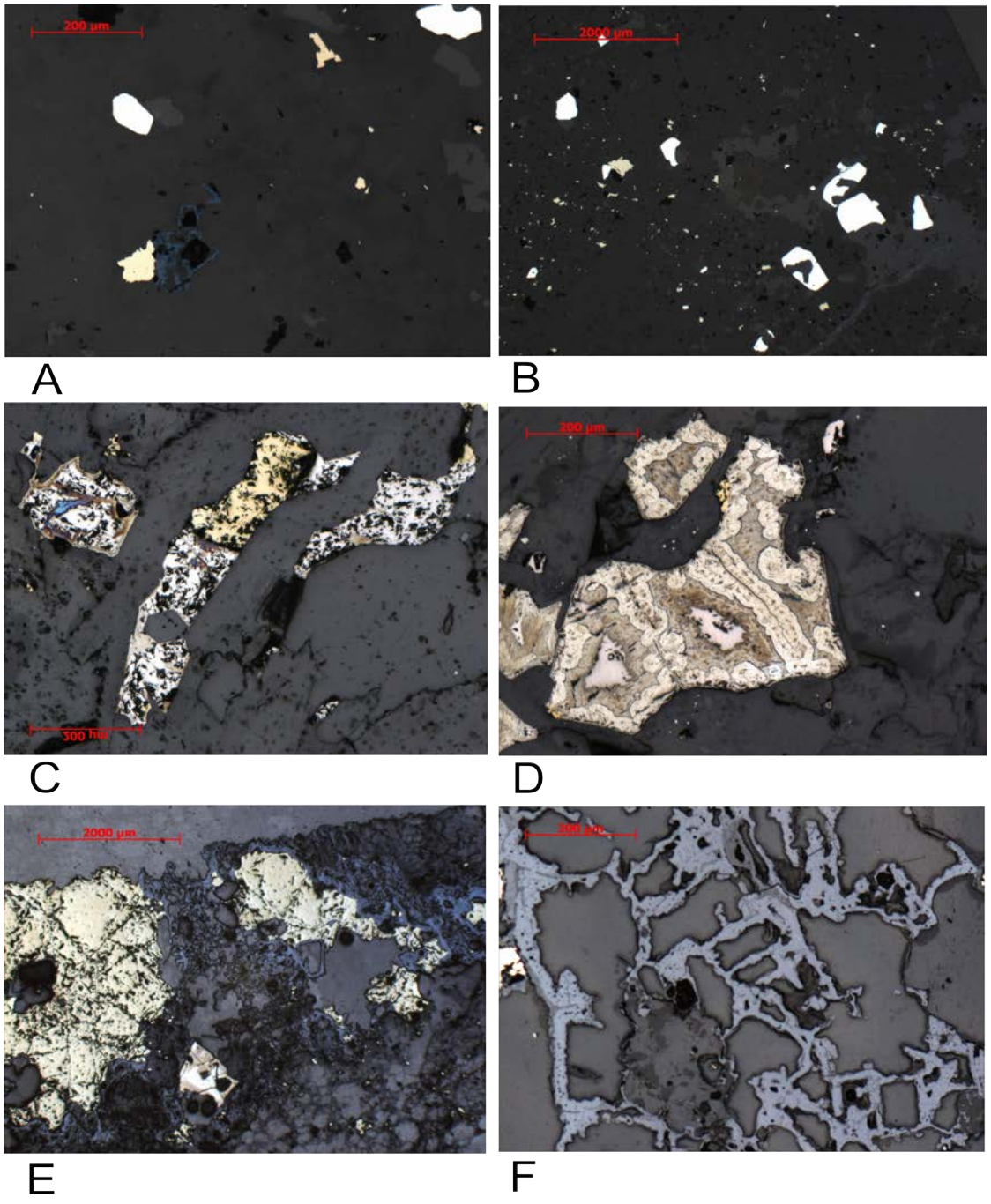

Figure 14. *Reflected light photomicrographs of ore minerals.* ***A+B****. Disseminated sulphides in sample 497608; pyrite (white), pyrrhotite (cream) and covellite (blue).* ***C****. Paragenesis of sulphides and silicates in sample 497611; pyrrhotite (cream), chalcopyrite (yellow), covellite (blue) and biotite (dark grey), the latter having a hexagonal shaped grain within a pyrrhotite grain.* ***D****. Sample 497610: Pyrrhotite (areas in the centre of the grain) altered to marcasite along fractures and grain edges. Marcasite forms characteristic "bird's-eye" texture.* ***E****. Sample 497610: Goethite (bluish grey) forming boxwork textures after alteration of sulphides; chalcopyrite (yellow) and pyrrhotite (cream, bottom centre).* ***F****. A closer look at the characteristic boxwork textures formed by goethite in sample 497610.*

5.2.2 XRD analysis results

The mineral assemblage established in the samples from the XRPD patterns as well as from one SXRD result is displayed in Table 2. The number of patterns per sample is given in column two. The XRPD patterns can be found in Appendix B, and these are named with the sample plus a number referring to the batch from the mineral separation lab (e.g. 497605-4).

Sample	No. of XRD pattern	Mineral assemblage
497605	3	quartz, albite, biotite, almandine-pyrope, ilmenite
497606	2	quartz, anorthite, clinochlore, spessartine, Mg-hornblende
497607	3	quartz, albite, biotite, almandine, Mg-hornblende, ilmenite
497608	3	quartz, albite, muscovite, goethite, chalcopyrite, pyrite, pyrrhotite, covellite
497609	1	quartz, albite, biotite, spessartine, Mg-hornblende, chalcopyrite
497610	2	quartz, albite, biotite, magnetite, chalcopyrite, pyrite
497611	3	quartz, albite, biotite, Mg-hornblende, spessartine, silimanit, chalcopyrite, pyrite, pyrrhotite, sphalerite
497612	2	quartz, albite, biotite, magnetite, ilmenite
497613	5	quartz, albite, biotite, almandine-spessartine, magnetite, ilmenite, pyrite

Table 2. *An overview of the minerals recognized in the samples by XRD analyses.*

All the samples contain quartz as well as plagioclase. Plagioclase is a calcian albite, except for sample 497606 wherein a sodian anorthite is recognized. It should be mentioned that the plagioclase phase recognized in the samples is chosen on the basis of the best fit between the sample pattern and the standard pattern, but due to the solid solution series of plagioclase a Rietveld refinement should be run to obtain a more perfect match. Mica pre-

sent in the samples is mostly biotite but muscovite is identified in sample 497608. One sample (497606) contains the clay mineral clinochlore (chlorite). The amphibole recognized in samples 497606, 497607, 497609 and 497611 is a magnesium-rich hornblende. Furthermore, silimanite is identified in sample 497611.
The garnets identified in the samples are from the pyralspite group being pyrope, almandine and spessartine. In general, it is difficult to determine precisely what garnet phase is present in the samples due to the solid solution between the three end-members, which gives very similar standard patterns. Sample 497607 contains almandine and samples 497606, 497609 and 497611 contain spessartine. Sample 497613 has a pattern that lies in between the standard patterns of almandine and spessartine. The results after a Rietveld refinement run display ~2% almandine, 85% spessartine, ~6% biotite, ~3% albite and ~4% quartz. Hence, the garnet in sample 497613 is mainly spessartine with a minor amount of the almandine phase. The XRPD pattern of batch 4 of sample 497605 shows a nearly clean sample of garnet with minor amounts of quartz. The standard patterns for almandine and pyrope are equally suited to fit the sample pattern. SXRD analysis on a crystal from sample 497605 batch 4 gives a cubic crystal lattice with a unit cell parameter of 11.5317 with a standard deviation of 0.007. Running the result in the software program “FindIt” almandine came out as the possible mineral.
Sulphides are identified in five samples. Chalcopyrite is identified in samples 497608, 497609, 497610 and 497611. Pyrite is recognized in samples 497610, 497611 and 497613 being the only identified sulphide in sample 497613. Pyrrhotite is identified in samples 497609 and 497611. Additionally, sphalerite is recognized in sample 497611 and covellite in sample 497608.
Magnetite and ilmenite are the only two oxides identified. Magnetite is recognized in samples 497610, 497612 and 497613. Additionally, the latter two contain ilmenite. In samples 497605 and 497607 ilmenite is recognized. The alteration product goethite is identified in sample 497608.

5.2.3 Microprobe analysis results

Garnet grains in sample 497605 and 497609 were analysed by WDS in the electron microprobe. Raw and calculated data as well as backscatter images and microphotographs of the grains showing the labelling can be found in Appendix C.

The average garnet composition in sample 497605 (A-F, Table 3.) is X_{Fe} 2.02; X_{Mg} 0.78; X_{Ca} 0.16 and minor Mn and Cr (0.02 and 0.01 respectively) giving a formula of $(Fe_2Mg_{0,8}Ca_{0,2})Al_2(SiO_4)_3$. No zoning is observed in the backscatter images which is consistent with the very similar results of analyses of the different grains. In sample 497609 the results exhibit an average composition of X_{Fe} 1.80; X_{Mg} 0.31; X_{Ca} 0.54; X_{Mn} 0.39 and minor Cr (0.01). Zoning is not registered in either the analyses results or in the backscatter image. The garnet formula is $(Fe_{1.8},Mg_{0.3}Ca_{0.5}Mn_{0.4})Al_2(SiO_4)_3$.

	497605A	497605B	497605C	497605D	497605E	497605F	497609
Weight %							
SiO2	38.90	38.58	38.82	39.12	39.19	38.76	38.60
Al2O3	21.92	21.80	21.91	22.23	22.11	21.81	21.30
FeO	31.78	31.45	30.68	30.74	31.34	31.76	27.70
MnO	0.33	0.18	0.29	0.40	0.34	0.31	5.80
MgO	6.73	6.33	7.21	7.42	7.49	7.12	2.70
CaO	2.03	2.61	1.82	1.64	1.51	1.60	6.40
TiO2	0.01	0.05	0.01	0.01	0.02	0.02	0.03
Cr2O3	0.07	0.10	0.10	0.07	0.20	0.03	0.10
Total	101.77	101.10	100.83	101.61	102.20	101.41	102.63
a (Å)	11,5317	11,5317	11,5317	11,5317	11,5317	11,5317	NA
	Numbers of ions on the basis of 12 OO						
Si	2.998	2.995	3.003	3.000	2.995	2.994	3.006
Al	1.991	1.995	1.998	2.009	1.992	1.986	1.959
Fe	2.048	2.042	1.985	1.972	2.003	2.052	1.804
Mn	0.022	0.012	0.019	0.026	0.022	0.020	0.384
Mg	0.771	0.731	0.830	0.846	0.852	0.818	0.311
Ca	0.168	0.217	0.151	0.134	0.124	0.132	0.536
Ti	0.000	0.003	0.000	0.001	0.001	0.001	0.002
Cr	0.004	0.006	0.006	0.004	0.012	0.002	0.006
	Mol per cent end-members						
Almandine	67.8	67.8	66.5	66.2	66.7	67.4	55.8
Grossular	5.4	7.0	4.7	4.3	3.5	4.4	18.9
Pyrope	25.9	24.5	27.8	28.4	28.5	27.5	11.2
Spessartine	0.7	0.4	0.6	0.9	0.7	0.7	13.7
Uvarovite	0.2	0.3	0.3	0.2	0.6	0.1	0.3

Table 3. *Results from the WDS analyses on the EMPA for sample 497605 and 497609 showing the chemical composition of garnet and recalculated end-member components following Rickwood (1968).*

The molecular percentage of the garnets' end-member components has been calculated following Rickwood (1968) (Detailed Instructions for Recalculation of Garnet Analyses into End-Member Molecules by the Proposed Scheme). Due to the fact that the EMPA can not distinguish between Fe^{2+} and Fe^{3+} all the iron has been reported as FeO which sets some limits to the recalculation scheme. The results are shown in table 3 and the full calculation

scheme plus explanations to the limits mentioned above can be found in detail in Appendix C.
All the garnets are of the pyralspite group although all of the grains contain some amount of the grossular end-member of the ugrandite group. The average composition for garnet in sample 497605 is $Alm_{67}Gro_5Pyr_{27}Sp_1$. Sample 497609 has important amounts of the grossular molecule, and the composition is $Alm_{56}Gro_{19}Pyr_{11}Sp_{14}$. Following Deer et al. (1992), the name is assigned according to the dominant 'molecular' type present, thus all of the garnets are almandine.

5.2.4 Major and trace elements

A table displaying data for selected major and trace elements including REE detected in the samples along with the calculated europium anomaly, the chondrite normalized La/Sm, Gd/Yb and La/Yb values can be found in Appendix D along with the raw data from the analyses made by AGC and Jørgen Kystol (GEUS).

Six samples have interesting metal concentrations. They are all auriferous. Sample 497608 has the highest Au concentration of 8160 ppb, as well as the highest Ag, As and Cu concentrations of 8 ppm, 7 ppm and 4585 ppm, respectively. Sample 497609 has concentrations of 1540 ppb Au, 2 ppm Ag, 2 ppm As and 107 ppm Cu. Sample 497610 has a 2470 ppb Au, 3 ppm Ag, 3 ppm As plus 716 ppm Cu content. The sample with the second highest copper concentration is sample 497611 with 1518 ppm Cu and 819 ppb Au, 2 ppm Ag and 4 ppm As. A distinct Au-Cu correlation is evident from Figure 15. Tellurium was measured only in sample 497608 due to its high Au concentration and gave a Te concentration of 1.1 ppm.

A spider diagram (Figure 16) shows the analyzed concentrations (ppm) of selected mobile (Rb, Ba, Sr, and K) and immobile elements normalized to N-MORB (Hofmann 1988). The samples show some trends: (1) high enrichment in Rb, Ba, K, and Pb relative to MORB, (2) Negative Nb and Ta anomalies, (3) variation in Sr concentrations, and (4) great variation in Cr concentrations from highly positive to highly negative anomalies. The pattern for sample 497608 is abnormal due to its strongly negative Ti anomaly, low concentration of Zr and Hf and positive Eu anomaly. Sample 497606 deviates from the general trend of the other patterns in a lower concentration of Rb, Ba and K.

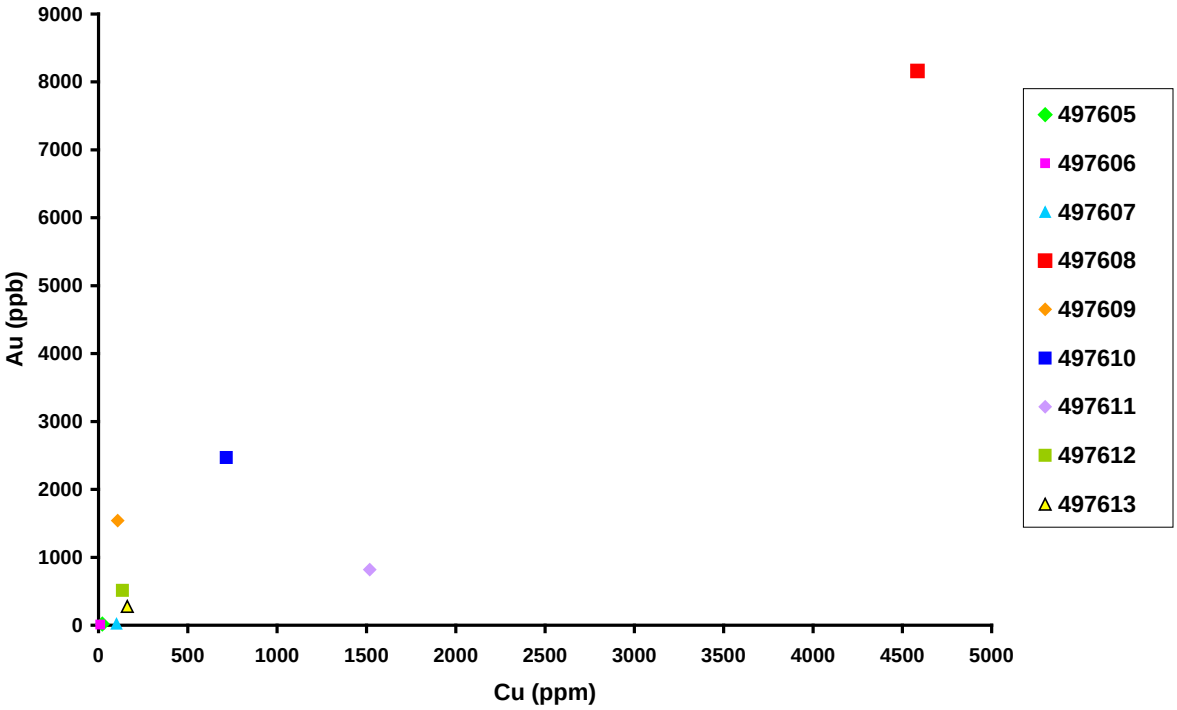

Figure 15. *Diagram showing the connection between copper (ppm) and gold (ppb) in the samples. The triangles represent the auriferous samples.*

5.2.5 Rare earth elements (REE)

All REE analyses are made on a whole rock material and the measured concentrations (ppm) are normalized to CI Chondrite (Anders and Grevesse 1989). In general, the samples show variable patterns (Figure 17). However, samples 497603 and 497606 show very similar patterns. The patterns are fairly flat (La/Yb_N = 1.88 and 1.67 respectively) with small negative europium anomaly (Eu/Eu* = 0.77 and 0.76 respectively). Most of the remaining samples have highly fractionated LREE-enriched patterns with La/Sm_N = 2.43-4.34 and comparatively flat HREE (Gd/Yb_N = 0.96-2.73). All but one sample have negative europium anomaly with Eu/Eu* = 0.25-0.87. Sample 497608 has a positive europium anomaly with Eu/Eu* = 2.46.

Two samples have a somewhat different pattern compared to the other samples. Sample 497613 displays a pattern with slight LREE depletion and increasing HREE proportion (Gd/Yb_N = 0.72). Sample 497607 has a very small negative europium anomaly (Eu/Eu* = 0.87).

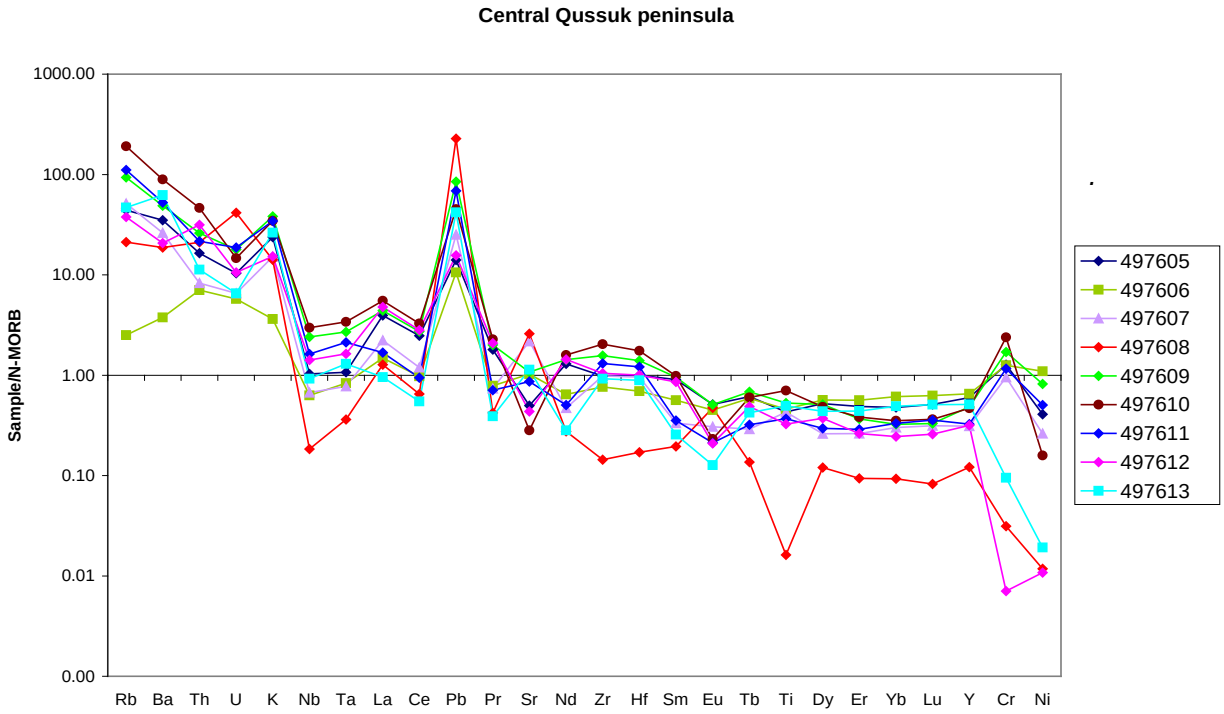

Figure 16. *Spider diagram showing N-MORB normalized patterns for whole rock samples 497605-497613 from the central part of the Qussuk peninsula.*

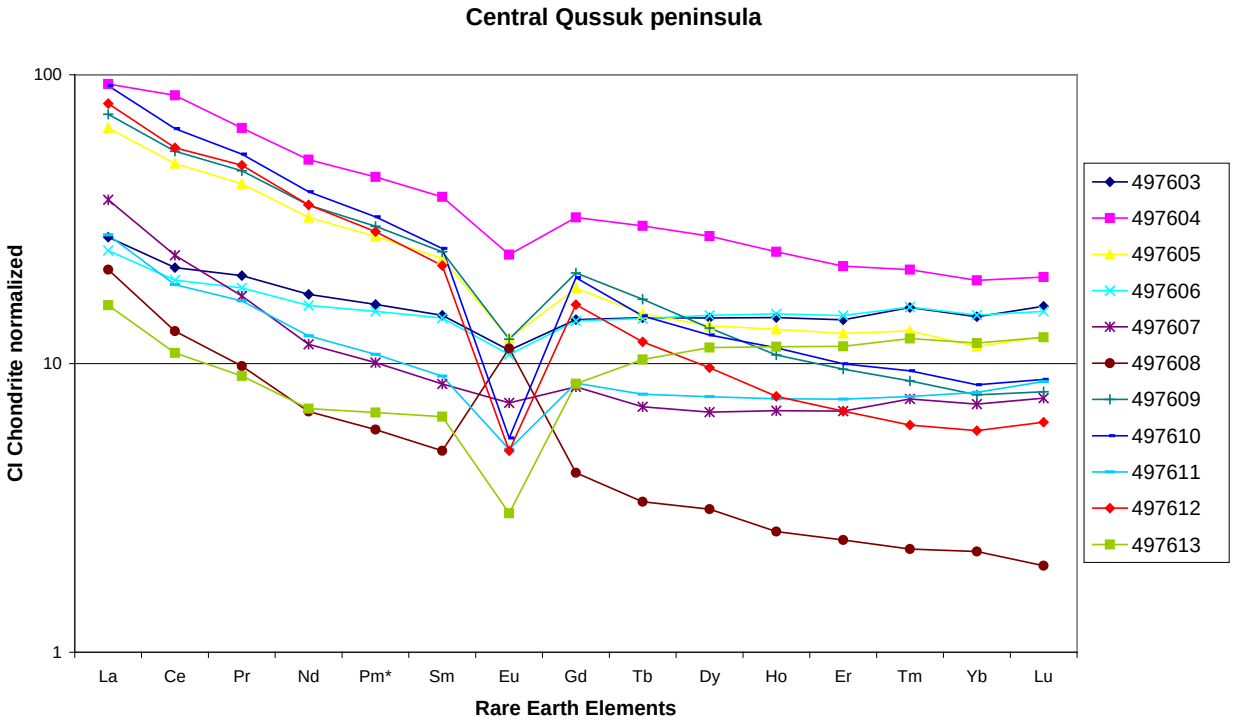

Figure 17. *REE CI normalized patterns for whole rock samples 497603-497613 from the central part of the Qussuk peninsula.*

5.3 Auriferous profile at north-western Qussuk peninsula

5.3.1 Profile line

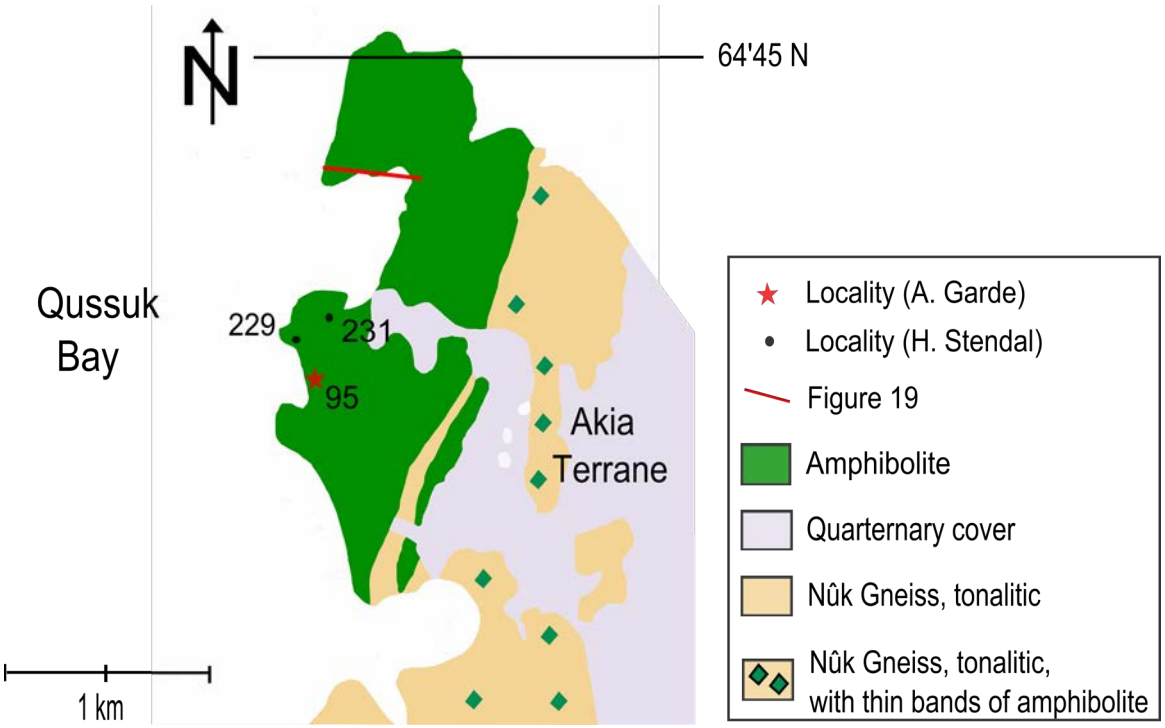

Figure 18. *West coast of the Qussuk peninsula showing the distribution of the supracrustals as well as the Nûk gneiss. Localities HST 229 and 231 are shown with a dot. A.A. Garde's locality 95 from 2004 is shown with a red star. The location of the profile of the northern side of the bay (see Figure 19) is marked by a red line.*

Anomalous gold concentration of 5.1 ppm was found in the north-western part of the Qussuk peninsula. The area is divided by a small bay (Figure 18). Five samples (497685 to 497689) were collected on the southern side of the bay between localities HST 229 with bearings N 64°43.963', W 51°06.491' and locality HST 231 with bearings N 64°43.997', W 51°06.312'. Garde's locality 95 from 2004 is marked with a red star. At this locality Garde sampled a rock with 0.2 ppm Au (Hollis et al. 2004). From the five samples, six polished thin sections, 18 XRPD patterns and five REE patterns form the basis for the rock descriptions. Detailed mineralogical descriptions can be found in Appendix A.
The profile of the northern side of the bay (Figure 19) represents the sequence where the samples were collected. Only one rock collected in the western part of the Qussuk is auriferous. However, in 2006 Nunaminerals A/S made a gold-find of 21 ppm which is marked on Figure 19 (Stendal, pers.comm.).

Figure 19. *The c. 200 m long sequence of banded amphibolite with several rust altered layers. The red star marks where Nunaminerals A/S found 21 ppm Au in an amphibolite layer. The picture is taken of the area north of the bay which represents the area south of the bay where the samples were collected.*

The area is a c. 200 m long sequence of N-S trending layered amphibolite with several rust altered horizons and cross-cutting granitic intrusives. In the most western part of the area a c. 25 m wide layer of mafic amphibolite is located (HST 229). The layer (sample 497685) is cut by numerous granitic intrusives of up to 1 m in width, and several cm wide layers of boudinaged calc-silicates are found (Figure 20A+B). The sample contains minor sulphides and oxides.

Figure 20. ***A.*** *c. 25 m wide layer of mafic amphibolite. A. Numerous granitic intrusives up to 1m in width cut the mafic amphibolite.* ***B.*** *Calc-silicate boudins of centimetre size in the mafic amphibolite.*

Samples 497686, 497687, 497688 and 497689 are collected in a c. 50 m wide unit of banded amphibolite with several siliceous rust altered layers. Samples 497686 and 497687 are from the same rust altered, sulphide-rich amphibolite layer c. 5 m wide (Figure 21A). Sample 497686 contains semi-massive sulphides of up to 25%. The sulphides are anhedral and rounded disseminated, fine to coarse grained pyrrhotite associated with fine to medium grained chalcopyrite and pyrite. Some of the pyrrhotite grains are >5 mm in diameter, and all grains show replacement by marcasite along fractures and grain edges. Sample 497687 contains ~20% disseminated fine to very fine grained anhedral pyrrhotite, pyrite and marcasite. A band of mafic amphibolite (sample 497688), up to 1 m wide, lies next to a quartz-rich, rust altered rock. The mafic amphibolite is cut by several coarse grained plagioclase veins ~1-40 cm in width (Figure 21B). Sample 497689 represents a garnetiferous orthoamphibole-cordierite gneiss with very coarse garnet phenocrysts of up to 10 cm in diameter (Figure 21C+D) which is located next to the mafic amphibolite.

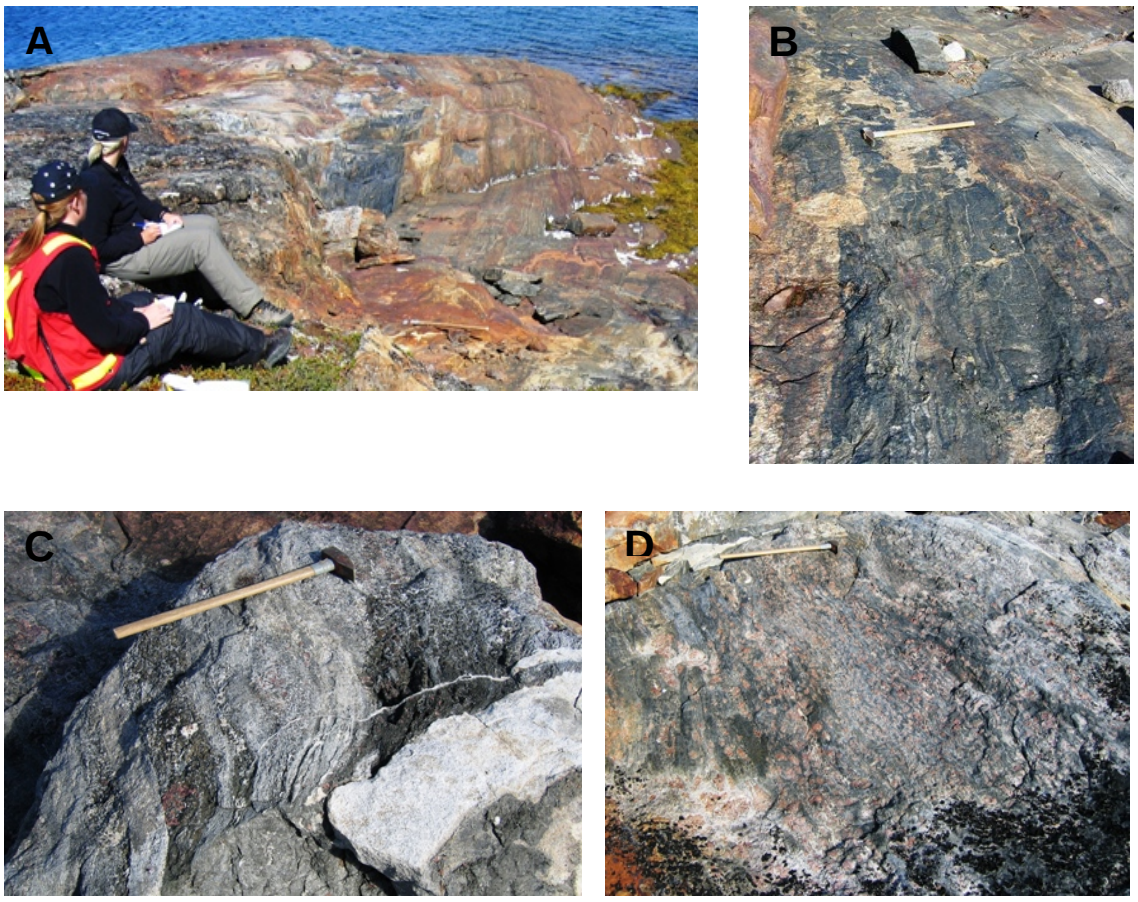

Figure 21. ***A****. A c. 5 m wide rust altered amphibolite layer rich in disseminated and semi-massive sulphides (samples 497686 and 497687).* ***B.*** *A mafic amphibolite layer up to 1 m in width cut by several plagioclase veins of varying sizes.* ***C****. A garnetiferous amphibolite (sample 497689) with a c. 5x10 cm large garnet cluster.* ***D****. Multiple coarse garnet grains of up to 5 cm in diameter in the grey garnetiferous amphibolite.*

5.3.2 XRD analysis results

Minerals recognized in the samples from the XRPD patterns as well as from two SXRD results are presented in Table 4. The number of patterns per sample is given in column two. The XRPD patterns can be found in Appendix B, and they are named with the sample plus a number referring to the batch from the mineral separation lab (e.g. 497685-6).

Quartz is recognized in all the samples with the exception of sample 497685. Anorthite is recognized as the plagioclase phase in all the samples but one (sample 497688), which contains a calcian albite. Mica is present in samples 497687, 497688 and 497689 as biotite.
Garnet is only recognized in one sample (497689). The SXRD result gave a unit cell dimension of 11.5032 with a standard deviation of 0.007 and running the result in the software program “FindIt” gives almandine as the possible mineral. However, in the powder pattern (497689-1-garnet) it is difficult to determine if the standard pattern for almandine or pyrope is the best fit.
The amphibole phase present in samples 497685, 497686 and 497688 is a magnesium-rich hornblende. Anthophyllite is identified as the amphibole in sample 497689.
Pyroxenes are present in samples 497685, 497686 and 497687. Augite-hedenbergite is recognized in samples 497686 and 497687. SXRD is used to identify the pyroxene in sample 497685 and gives an orthorhombic unit cell dimension value of a: 18.3140 (0.0018), b: 8.8699 (0.0006), c: 5.2129 (0.0005) with the standard deviations given in the brackets. The result run in “FindIt” gives enstatite as the possible mineral.
The Mg-Al-silicate cordierite is identified in sample 497689 and possibly in sample 497686.
The oxides present are magnetite, ilmenite and hematite, all three identified in sample 497689. Samples 497685 and 497687 contain magnetite.
Several sulphides are recognized in all the samples but one (497688). Sample 497685 contains chalcopyrite, covellite and probably galena. Chalcopyrite, pyrrhotite, marcasite and sphalerite are recognized in sample 497686. Identified in sample 497687 are pyrite, pyrrhotite, marcasite, covellite and possibly pentlandite. Sulphides present in sample 497689 include chalcopyrite and pyrite.
The patterns of sample 497685 show that it has a fairly extensive mineral assemblage. In addition to the above mentioned minerals in the sample, the copper-selenide krutaite has been identified. Another sample with a widespread mineral assemblage is sample 497689 with 12 minerals identified by XRD.

Sample	No. of XRD pattern	Mineral assemblage
497685	4	anorthite, Mg-hornblende, enstatite-ferrosilite, magnetite, chalcopyrite, galena, covellite, krutaite
497686	5	quartz, anorthite, Mg-hornblende, augite-hedenbergite, cordierite (?), chalcopyrite, pyrrhotite, marcasite, sphalerite
497687	3	quartz, anorthite, biotite, augite, magnetite, pyrite, pyrrhotite, marcasite, pentlandite
497688	3	quartz, albite, biotite, Mg-hornblende
497689	3	quartz, anorthite, biotite, anthophyllite, almandine-pyrope, cordierite, magnetite, ilmenite, hematite, chalcopyrite, pyrite,

Table 4. *An overview of the minerals identified in the samples by XRD analyses.*

5.3.3 Microprobe analysis results

Three garnet grains in sample 497689 were analyzed by WDS in the electron microprobe resulting in seven analyses displayed in Table 5. Raw and calculated data as well as microphotograph and backscatter image can be found in Appendix C. The results are almost identical hence giving an average composition of X_{Fe} 1.76; X_{Mg} 1.10; X_{Ca} 0.11 and minor Mn (0.05). The very similar results are consistent with the fact that no zoning is observed on the backscatter image. The chemical formula of the garnet in sample 497689 is $(Fe_{1.8}Mg_{1.1}Ca_{0.1})Al_2(SiO_4)_3$.

The garnet end-member components have been calculated following Rickwood (1968) (Detailed Instructions for Recalculation of Garnet Analyses into End-Member Molecules by the Proposed Scheme). All the iron has been reported as FeO because the EMPA can not distinguish between Fe^{2+} and Fe^{3+} and it results in some limits to the recalculation scheme pointed out in the appendix. The results are shown in table 5 and the full calculation scheme can be found in detail in Appendix C.
The average composition of the garnet is $Alm_{58}Gro_4Pyr_{36}Sp_2$ naming it almandine by following Deer et al. (1982). The garnet is a member of the pyralspite group.

	497689A	497689B	497689C
Weight %			
SiO2	39.99	39.86	40.08
Al2O3	22.70	22.62	22.58
FeO	28.58	27.81	27.84
MnO	0.91	0.80	0.81
MgO	9.78	9.83	9.82
CaO	1.33	1.37	1.38
TiO2	0.00	0.01	0.00
Cr2O3	0.04	0.03	0.01
Total	103.33	102.33	102.51
a (Å)	11,5032	11,5032	11,5032
	Numbers of ions on the basis of 12 O		
Si	2.984	2.993	3.003
Al	1.996	2.002	1.993
Fe	1.783	1.746	1.744
Mn	0.057	0.051	0.051
Mg	1.085	1.098	1.094
Ca	0.107	0.110	0.110
Ti	0.000	0.000	0.000
Cr	0.002	0.002	0.001
	Mol per cent end-members		
Almandine	58.1	57.9	57.9
Grossular	3.5	3.6	3.7
Pyrope	36.4	36.8	36.6
Spessartine	1.9	1.7	1.7
Uvarovite	0.1	0.1	0.0

Table 5. *Results from the WDS analyses on the EMPA for sample 497689 showing the chemical composition of garnet and the recalculated end-member components following Rickwood (1968).*

5.3.4 Major and trace elements

Data for selected major and trace elements including REE detected in the samples along with the calculated europium anomaly, the chondrite normalized La/Sm, Gd/Yb and La/Yb values can be found in Appendix D as well as the raw data. The results are obtained from the analyses made by AGC and Jørgen Kystol, GEUS.

The concentrations of metals such as Au, Ag, Cu, Ni, Co and Zn can be found in Appendix D. The only auriferous sample is 497686 with 5100 ppb Au. This sample has a silver con-

centration of 1 ppm not different from sample 497687, which only show 88 ppb Au. Sample 497686 is enriched in copper with 3708 ppm compared to the other samples with concentrations between 5-434 ppm Cu (Figure 22). No major variations in Ni, Co and Zn concentrations are seen in the samples. Tellurium was measured only in sample 497686, due to the high Au content, and gave a concentration of 1.2 ppm.

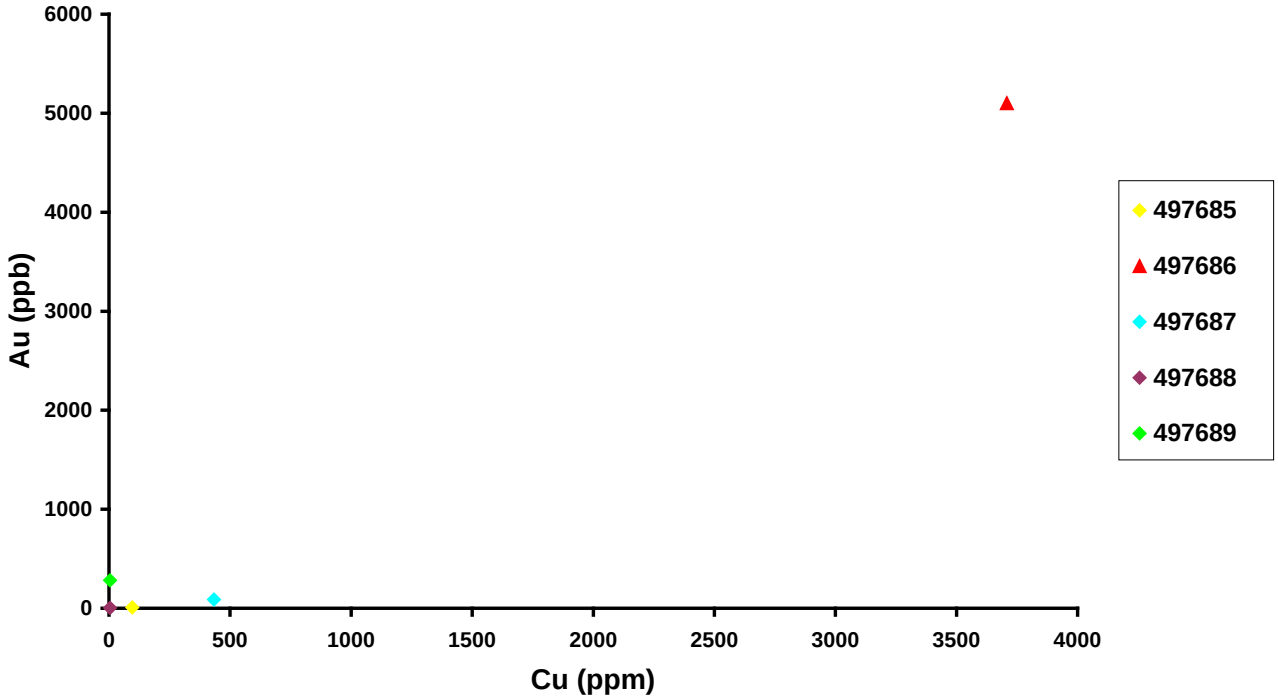

Figure 22. *The correlation between Cu (ppm) and Au (ppb) concentrations. The auriferous sample (497686) is marked by a triangle. It is evident that the only sample containing significant amount of copper is also the only sample with a gold content.*

Selected large-ion-lithophile (LIL), high-field-strength (HFS) and other immobile elements' concentrations are shown in a spider diagram (Figure 23). The measured concentrations (ppm) are normalized to N-MORB (Hofmann 1988). The samples show very varied patterns except for Pb enrichment relative to MORB and negative Nb and Ta anomalies are seen in all the patterns. Great variation in Cr concentrations is seen in the samples. Sample 497686 shows a pattern with strong negative Ti anomaly and strong positive Eu anomaly. Sample 497685 shows a somewhat comparable trend to that of sample 497686 apart from the mobile elements (Rb, Ba, Th, U, and K).

5.3.5 Rare earth elements (REE)

All REE analyses are made on a whole rock material and the measured concentrations (ppm) are normalized to CI Chondrite (Anders and Grevesse 1989). The samples display very different patterns (Figure 24). Sample 497685 has a HREE over LREE enriched pattern with La/Yb_N = 0.50 and a small positive europium anomaly of Eu/Eu* = 1.11. Samples 497687, 497688 and 497689 show highly fractionated patterns with LREE-enrichment and HREE-depletion (La/Yb_N = 5.37-9.02). Sample 497689 exhibit fairly flat HREE with a slightly concave curve. Samples 497687 and 497689 have prominent negative europium anomaly with Eu/Eu* = 0.54 and 0.45, respectively. Sample 497688 displays a minute positive europium anomaly (Eu/Eu* = 1.24). Sample 497686 exhibits a fairly flat pattern (La/Yb_N = 1.82) with a notable positive europium anomaly of Eu/Eu* = 1.68.

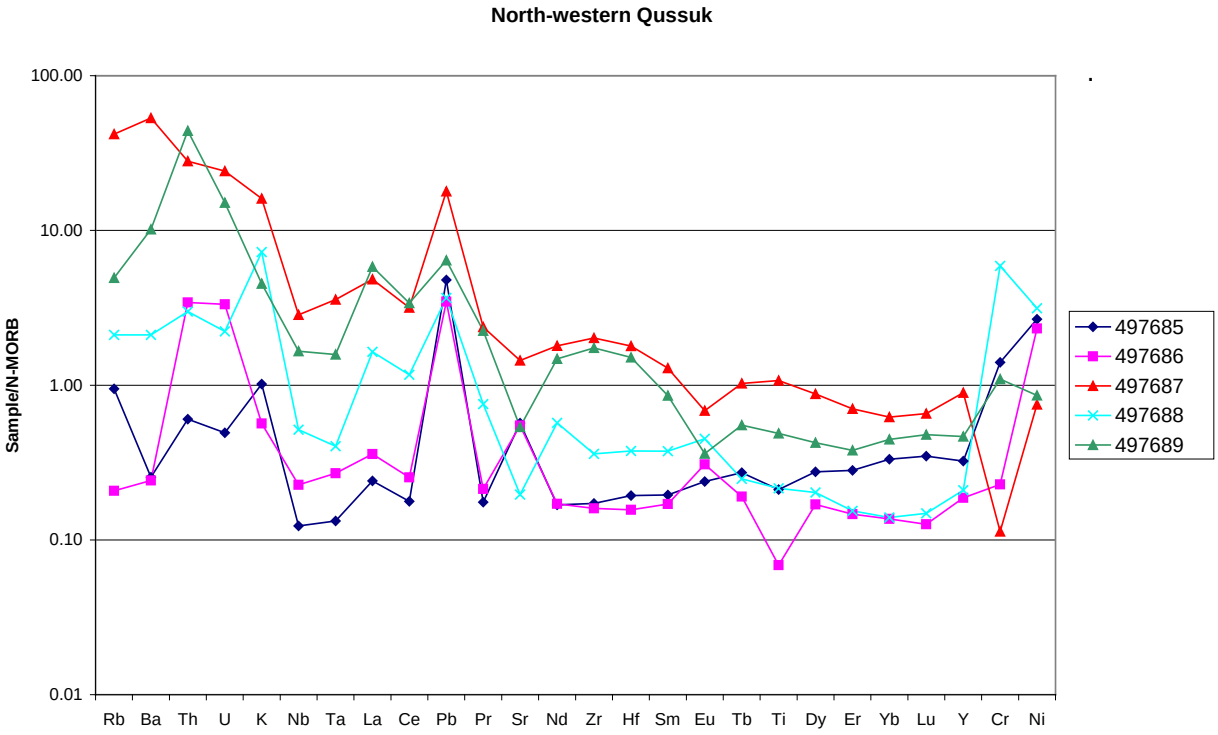

Figure 23. *Spider diagram showing N-MORB normalized patterns for whole rock samples 497685-497689 from the north-western Qussuk area.*

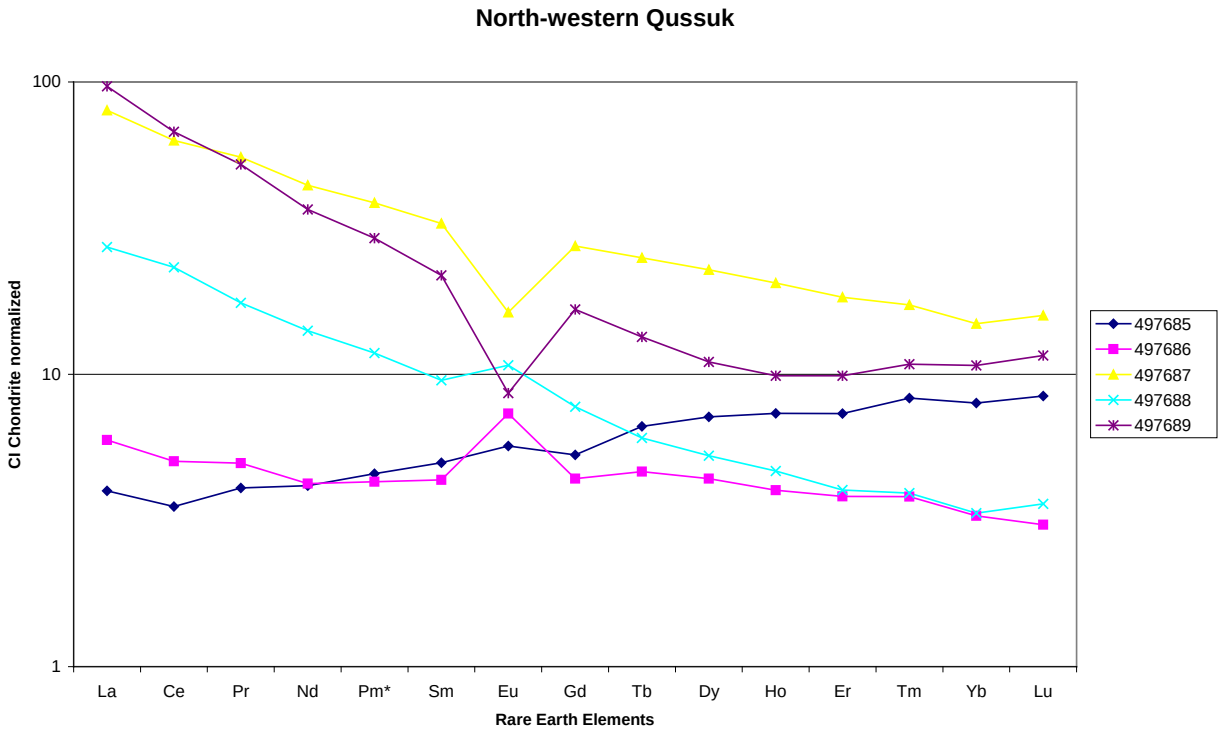

Figure 24. *REE CI normalized patterns for whole rock samples 497685-497689 displaying very different patterns.*

6. DISCUSSION

6.1 Geochemical characteristics

6.1.1 Rare earth element abundances

Chondrite normalized REE patterns (Figure 25B) of the supracrustal rocks collected in the central Qussuk peninsula can be divided into two main groups with the exception of three deviating samples namely 497607, 497608 and 497613. Group 1: two samples (497603 and 497606) exhibit almost identical fairly flat patterns with a small negative Eu anomaly. In the field they are observed as amphibolite s.s. due to their mafic appearance and a comparison with the patterns published by Garde (2007) shows a notable resemblance with sample 477345 (Figure 25A). Group 2: samples 497604, 497605, and 497609 to 497612 show highly fractionated LREE-enriched REE patterns increasing toward La with relatively flat HREE and prominent negative Eu anomalies. This group represents leucocratic amphibolites with or without disseminated sulphides and a garnetiferous schist with no sulphides. Comparison of these patterns with Garde's (2007a) patterns representing fragmental amphibolite with or without disseminated sulphides and volcano-sedimentary schist show there is a good correlation, but only a few of Garde's patterns show Eu anomalies (Figure 25A). Sample 497607 shows a similar LREE over HREE enriched pattern, but with a small Eu anomaly and a small concave curve in HREE between Gd and Tm. The sample represents a garnetiferous rock with no sulphide content. Sample 497608, a siliceous sulphide-mineralized rock with the highest Au concentration, shows a similar LREE enriched and HREE depleted pattern as the other sulphide-mineralized rocks, but it is more fractionated and has a prominent positive Eu anomaly. The latter feature is not seen in any of the data published by Garde (2007a). Sample 497613 representing a sulphide-bearing amphibolite has an abnormal REE pattern not comparable to any other samples in this thesis or data published by Garde (2007a).

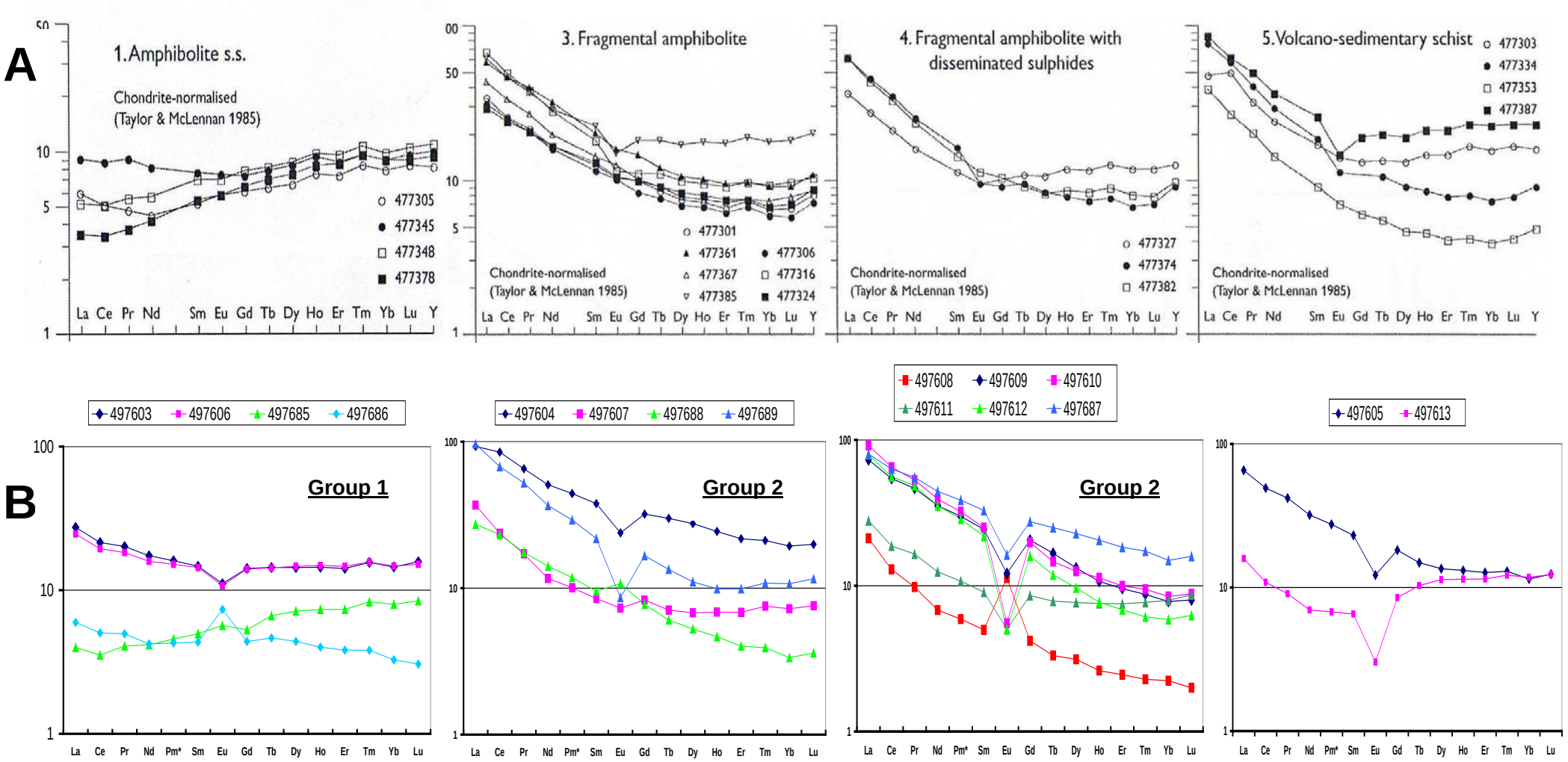

Figure 25. ***A****. Chondrite normalized REE patterns published by Garde (2007).* ***B****. CI normalized REE patterns of the samples collected for this thesis. Comparable patterns between published data and data for this thesis (from left to right): amphibolite s.s., fragmental amphibolite, fragmental amphibolite with disseminated sulphides and volcano-sedimentary schist. The patterns in general show good similarities although the negative Eu anomalies are much more prominent in the samples for this thesis and the two strong positive Eu anomalies in samples 497608 and 497686 are exceptional.*

Most of the supracrustal rocks from the north-western part of the Qussuk peninsula show REE patterns similar to those from the central part (Figure 25B). The pyroxene-amphibolite represented by sample 497685 is slightly depleted in LREE and shows a minute positive Eu anomaly, thus being somewhat different from any other sample. It resembles Garde's (2007a) amphibolite s.s. represented by sample 477378 (Figure 25A). Samples 497687, a sulphide-mineralized leucocratic amphibolite, and 497689, a garnetiferous anthophyllite-cordierite bearing gneiss, show strongly fractionated LREE-enriched patterns with sample 497687 showing slight HREE depletion and sample 497689 showing relatively flat HREE with a concave curve from Gd to Tm lowest at Ho and Er. Both samples show prominent negative Eu anomalies, and they can be compared to sulphide-mineralized samples in the central Qussuk peninsula and the fragmental amphibolite data published in Garde (2007a) (Figure 25A). Sample 497688 shows a similar fractionated REE pattern but with a small positive Eu anomaly. The sample represents a mafic amphibolite. The auriferous sulphide-mineralized siliceous rock represented by sample 497686 shows a fairly flat REE pattern with a prominent positive Eu anomaly. It can be compared to the amphibolite s.s. published by Garde (2007a) except from the positive Eu anomaly that is not seen in Garde's samples (Figure 25A).

The relatively flat REE patterns (sample 497603 and 497606) with very slightly enriched LREE and the somewhat LREE depleted pattern (sample 497685) are reminiscent of low-K tholeiites (Taylor et al. 1969). The highly fractionated REE patterns with LREE enrichment and fairly flat HREE have REE patterns comparable with those of calc-alkaline volcanics (Hess 1989). The pronounced negative Eu anomalies seen in the REE patterns with the highly fractionated REE abundances are another characteristic feature of andesites. The greater enrichment in LREE, and a progressively developing negative Eu anomaly from basalt to andesite, can be explained by separation of an assemblage of calcic plagioclase+augite+olivine, e.g. Mann (1983).
The small positive Eu anomaly that is seen in sample 497688 can be explained by the high content of plagioclase in accordance with Hess (1989). However, the REE patterns of the samples with the highest Au concentrations (samples 497608 and 497686) show strong positive Eu anomalies. The frequencies of negative Eu anomalies in Archaean volcanic rocks are significant. Therefore, it is assumed that the distribution of strong positive Eu anomalies seen in some of the rocks is not controlled by their volcanic components. Hence, these must be explained in a different way, which could very well be fluid/rock interaction controlled by hydrothermal alteration of the rock. Several authors have worked with REE behaviour of fluids (e.g. Lottermoser 1989, Bau 1991, Klinkhammer et al. 1994) and they all found that hydrothermal fluids are enriched in LREE and show a pronounced positive Eu anomaly when normalized to chondrite. The REE patterns of these fluids are very dissimilar from those of seawater and MORB which typically are LREE, Ce, and Eu depleted and HREE enriched (Lottermoser 1989; Klinkhammer et al. 1994) (Figure 26). Klinkhammer et al. (1994) suggest that the dominant process, setting the REE pattern of hydrothermal fluid, is ion exchange during the alteration of (hydrothermal) plagioclases. The suggestion is based on the conclusion that the LREE enriched patterns observed for hydrothermal fluids are related to the alteration of rock surfaces in contrasts to other writers' idea that complexation should be setting the REE patterns (e.g. Bau 1991). However, Klinkhammer et al. (1994) realize that the formation of the characteristic REE patterns for deep-sea fluids re-

quires the action of a selective process, as in REE ion exchange between fluids and crystals.

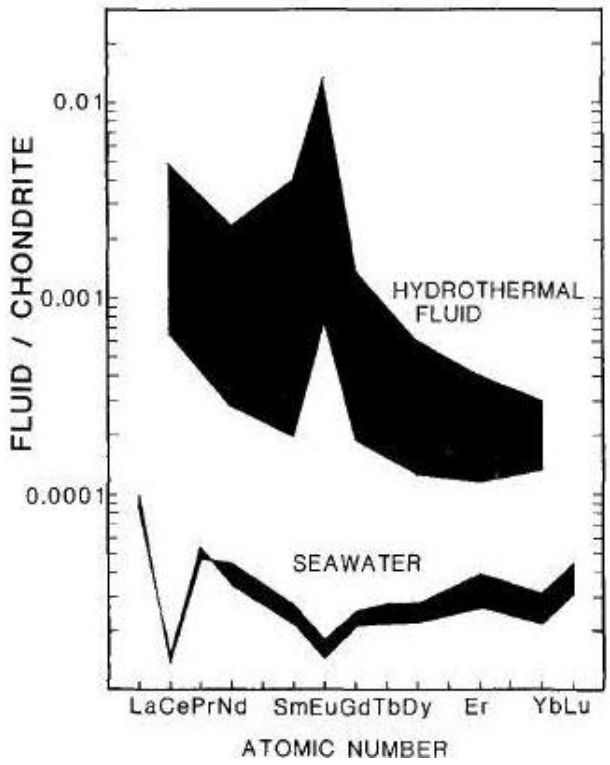

Figure 26. *Range of REE results on hydrothermal fluids of the East Pacific Rise and on seawater. From Lottermoser (1989).*

The An to Ab alteration sequence reported in hydrothermally altered plagioclase (e.g. Phinney and Morrison 1990) may have important consequences for REE partitioning between fluid and rock. The Eu content of tholeiitic basalt is directly related to the Ab content of the plagioclase component (Lagache and Dujon 1987) generated by the substitution of Eu^{2+} for Sr^{2+}. Albitization, which is the formation of hydrothermal plagioclase (albite), provides the substitution of Na and Sr for Ca, thus supplying an explanation for the prominent positive Eu anomaly observed in the two samples.
The correlation between sodium and gold in sample 497608 supports the suggestion that albitization has taken place (Figure 27). The concentrations are in whole rock material.

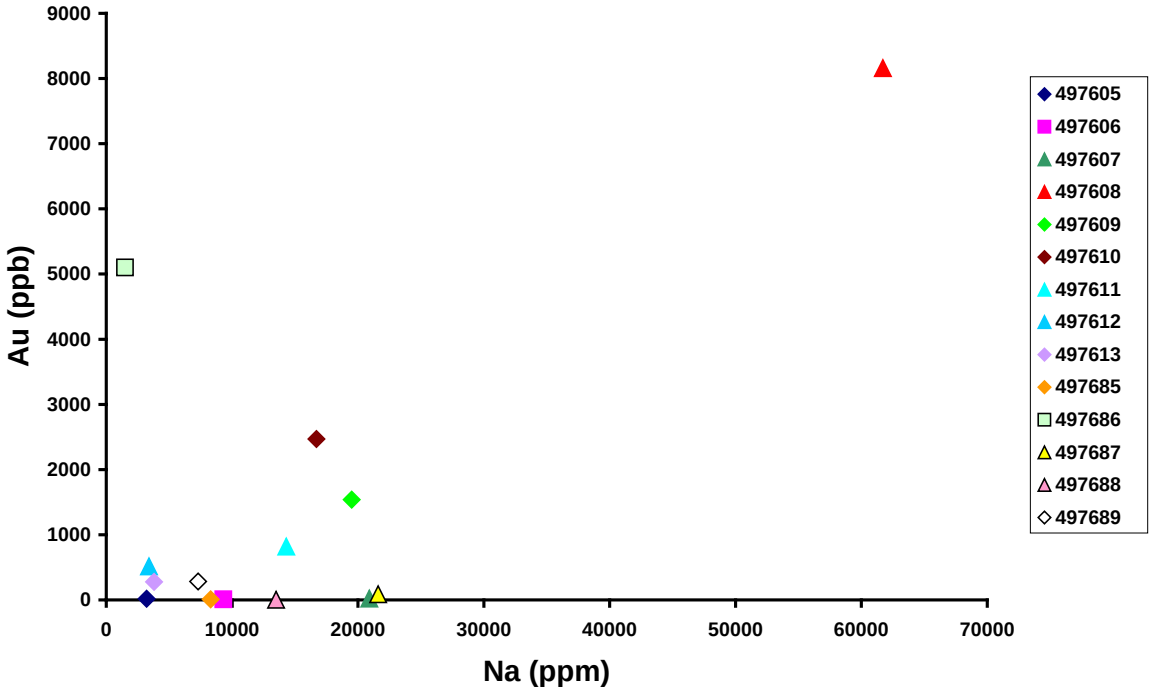

Figure 27. *Correlation between bulk concentrations of Au (ppb) and (Na) (ppm) in the supracrustal rocks. Albitization has taken place in the sample with the highest gold content (497608; 8100 ppb Au).*

6.1.2 Trace element abundances

N-MORB normalized spider diagram patterns (Figure 28B) of the samples from the central Qussuk peninsula (497603-497613) can be divided into two main groups, except for the pattern of sample 497608 which deviates somewhat. Group 1 (sample 497603 and 497606) has a relatively flat pattern. The two samples have very similar patterns with strong Pb enrichment, negative Nb and Ta anomalies, Sr enrichment and negative Eu and Ti anomalies. In LIL abundances the two patterns deviate from one another, where sample 497603 is highly enriched in Rb and Ba and sample 497606 is not. Group 2 has enrichment in LIL elements and Pb, relative negative Nb and Ta anomalies and depletion in HFS elements relative to LILE but more or less the same as MORB composition (~1). These features are all characteristic of andesites. However, the enriched and variable contents of LILE in the samples are unlikely to represent original compositions. According to Garde (1997; 2007a,b) the amphibolite-facies rocks received their present LILE patterns during peak metamorphism at c. 2980 Ma. The presence of relative negative anomalies for Nb and Ta in all the samples, as well as negative anomalies for Ti in some of the samples, is indicative of a subduction-related environment (Parlak et al. 2004). The patterns of group 1 are somewhat comparable to the patterns of amphibolite s.s. in Garde (2007a). The group 2 patterns are comparable to the data for fragmental amphibolite with or without disseminated sulphides published by Garde (2007a) except from the fact that the patterns published by Garde show decrease in HSFE (Figure 28A). Sample 497608 has a spider dia-

gram pattern with positive U anomaly, the highest enrichment of Pb and Sr of all samples, a concave curve from Nd to Eu compared with convex curves for the other samples and a profound negative Ti anomaly. The pattern cannot be compared to any of the data published in Garde (2007a).

The spider diagram patterns (Figure 28B) of the samples in the north-western Qussuk area (497685-497689) are all fairly different and show only two general trends: enrichment in Pb and relative negative Nb and Ta anomalies. Only the pattern for sample 497687 can be compared to the group 2 patterns from the central Qussuk peninsula and hence to the published data for fragmental amphibolite in Garde (2007a) (Figure 28A). The other patterns are too random for the scope of this thesis to be considered. A comparison of the spider diagram patterns of the two samples with the highest Au concentrations (497608 and 497686) shows that they display the same pronounced negative Ti anomaly and positive Sr and Eu anomalies, the latter being consistent with the REE data presented above suggesting an albitization of the rocks.

The typical geochemical features of calc-alkaline volcanics of island arc systems are fractionated LREE and almost flat HREE patterns, low TiO_2 wt%, high Al_2O_3 wt%, low Ni and Co, and Ni/Co ratios <1 and V/Ni ratios >10 (e.g. Peccerillo and Taylor 1976; Taylor et al. 1969b). The Ni concentrations of the supracrustal rocks from the central Qussuk peninsula range between 2-164 ppm; four samples (497604, 497608, 497612 and 497613) have 2-3 ppm Ni and the remaining seven samples have 24-164 ppm Ni. The calculated Ni/Co ratios range between <1 and <6, the samples with contents of 2-3 ppm Ni have Ni/Co ratios <1 correspondingly. The V/Ni ratios are between 1 and 51. The samples from the north-western Qussuk peninsula have very high Ni concentrations of 112-469 ppm, Ni/Co ratios between <4 and >8 and V/Ni ratios between <1 and 2. The high concentrations of Ni, Co and Cr (see table in Appendix D) as well as the inconsistent Ni/Co and V/Ni values do not support an andesitic origin of the supracrustal rocks from the north-western Qussuk area, and suggests that only the four rocks with Ni/Co ratios <1 are of andesitic affinity.
Ni and Cr are both highly compatible and are immobile during regional metamorphism therefore yielding the original pre-metamorphic concentrations. No record of Ni and Cr enrichment in volcanics due to hydrothermal alteration has been reported except in areas with very high Ni-sulphide precipitation. Thus, the high Ni and Cr concentrations in the samples presented in this thesis cannot be explained by pre-metamorphic hydrothermal alteration or regional metamorphism. Frei et al. (2002) have presented data suggesting that metabasalts from the Isua greenstone belt have gained their enrichment in certain trace elements from pre-metamorphic metasomatic alteration. The fluids were typically Th, U, LREE, Ba, Pb and alkaline rich (Frei et al. 2002). Possibly, a metasomatic alteration of a basaltic bulk composition could account for the LREE enriched REE patterns with relatively flat HREE, and the strong enrichment in LILE in the samples from the Qussuk area which would explain the high Ni and Cr concentrations.

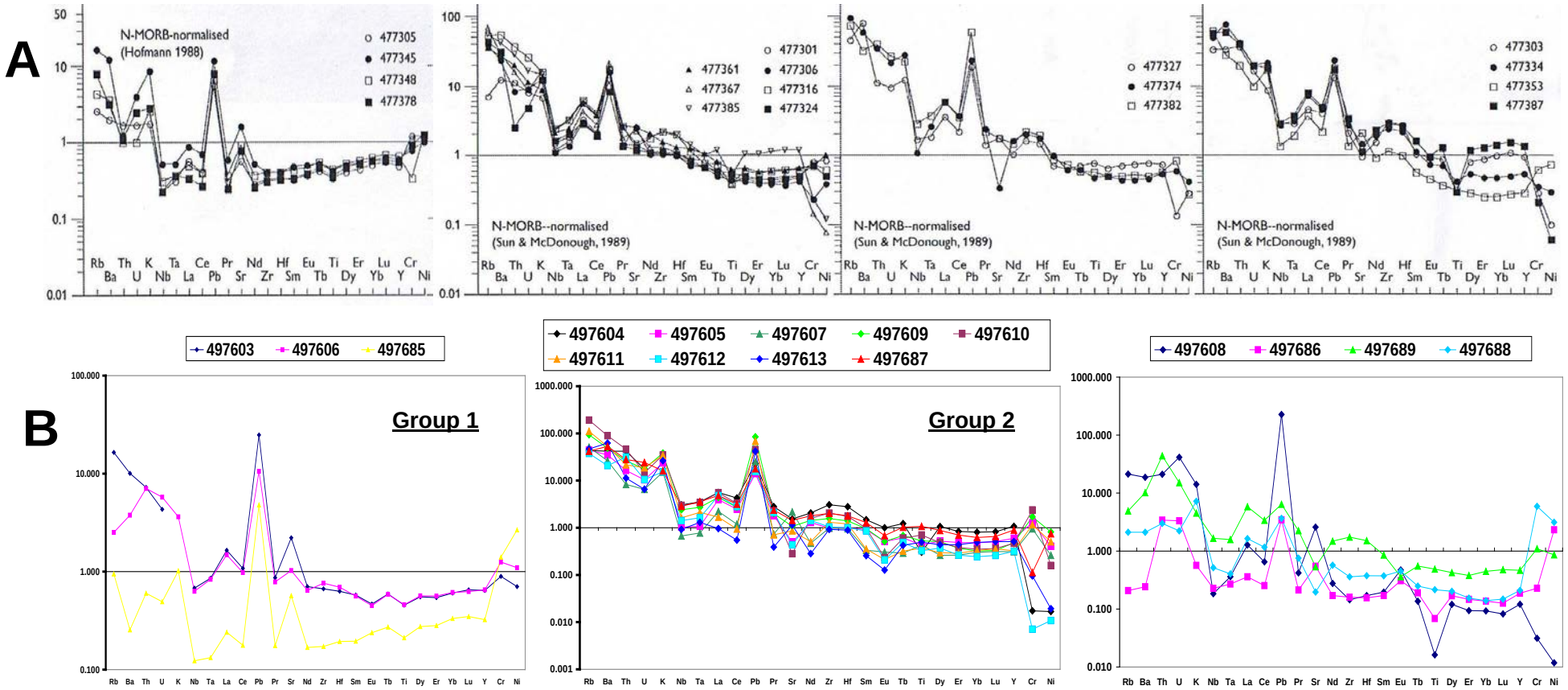

Figure 28. ***A.*** *N-MORB normalized spider diagrams published by Garde (2007) for (from left to right) amphibolite s.s., fragmental amphibolite, fragmental amphibolite with disseminated sulphides and volcano-sedimentary schist.* ***B****. For comparison: N-MORB normalized spider diagrams for samples collected for this thesis. Patterns of the samples in the two first diagrams (from the left) show similar patterns with the amphibolite s.s. and the fragmental amphibolite with or without disseminated sulphides, respectively. Patterns in the diagram to the right can not readily be compared to any of the data published by Garde (2007). The two samples with the highest Au content (497608 and 497686) show somewhat different patterns but with some similarities like pronounced negative Ti anomaly, and positive Eu anomaly.*

6.2 Metamorphism of the Qussuk Area

The supracrustal rocks of the Akia terrane in the north-western area of the Qussuk peninsula differentiate from the supracrustal rocks in the central part of the Qussuk peninsula by having pyroxene content. Pyroxenes are detected in three samples (497685, 497686 and 497687) by XRD but occur only in the thin sections of sample 497685 and 497686. Sample 497685 has a mineral assemblage of orthopyroxene + plagioclase + hornblende + opaque phases, the orthopyroxene being mostly enstatite with c. 10 % of the ferrosilite molecule. The orthopyroxene grains occur as poikiloblastic porphyroblasts (0.5-1 cm) enclosing anhedral plagioclase. Sample 497686 has a mineral assemblage of clinopyroxene+plagioclase+hornblende+quartz+opaque phases. Clinopyroxene is augite-hedenbergite based on the greyish colour of the clinopyroxene in thin section as well as an identification by XRPD. In both samples it is evident that the pyroxenes are being partly replaced by hornblende. Most of the hornblende grains are characteristically green, but the grains bordering the orthopyroxenes are greenish white and show both twins and exsolution lamellae. The colour variation is presumably due to different chemical compositions. Hence, the green hornblende is older than the light coloured hornblende, which is the last to replace the orthopyroxene grains, and therefore has a different chemical composition.

It is generally accepted that large parts of the Akia terrane have undergone granulite facies metamorphism and that the eastern part of the terrane, which spans north and east of Qussuk (thus, including the Qussuk peninsula), has been exposed to amphibolite facies metamorphism only (e.g. Garde 2007a). However, the presence of pyroxene in three samples of the north-western Qussuk peninsula as well as the poikiloblastic texture of the orthopyroxene grains indicate that at least part of the area has undergone granulite facies metamorphism according to the mineral assemblages diagnostic of the metamorphic facies, e.g. Yardley (1989): “Low pressure granulite facies metamorphosed metabasic rocks show a mineral assemblage of orthopyroxene + clinopyroxene + plagioclase hornblende olivine”. Furthermore, the different stages of hornblende replacing pyroxene indicate that the area has undergone retrogressive metamorphism to amphibolite facies.

Sample 497688 is a mafic amphibolite with a mineral assemblage of hornblende+plagioclase +quartz+biotite. It is found adjacent to sample 497687 and the ortho-amphibole-cordierite gneiss (sample 497689) described below in section 6.3.2. The latter as well as the hornblende-rich amphibolite are most likely metmamorphosed to amphibolite facies only, hence the rock unit succession described here may represent an area showing transitional metamorphic grades from granulite facies to amphibolite facies from west to east.

6.3 Mineral Assemblages and Alteration

6.3.1 Supracrustals from the central Qussuk peninsula

A greenstone is defined as a low-grade, regional metamorphic rock containing green minerals like actinolite, epidote and hornblende. Thus, the supracrustal rocks from the central Qussuk peninsula can be considered as greenstones, since the metamorphism in the area has only reached amphibolite facies and most of the rocks contain a certain amount of hornblende. Two samples were collected to represent hydrothermally unaltered amphibolite, sample 497603 representing mafic amphibolite sensu stricto and sample 497604 representing leucocratic amphibolite, the latter being the most abundant lithology in the area. The amphibolites have varying percentages of quartz+plagioclase+hornblende+biotite garnet oxides.

Three samples were collected in a thin band of variously altered mafic amphibolite (497605, 497606 and 497607). A garnetiferous biotite schist (sample 497605) with a mineral assemblage of garnet+biotite+plagioclase+quartz+oxides will be discussed in further detail in section 5.3.3, concerning the garnet composition and the structure of the unit. Sample 497606 is an amphibolite s.s. with a mineral assemblage similar to that of sample 497603. The mineral assemblage is amphibole+biotite+quartz+plagioclase+garnet+sulphides+chlorite. Compared to sample 497603 it has garnet and sulphide content, and it is the only sample containing minor chlorite, which is considered to be of retrograde origin. The amphibole phase is represented by two minerals. The dominating mineral is hornblende, and the other mineral, which is light coloured grains showing perfect cleavage and weak light green pleochroism, is possibly tremolite that is poor in iron. However, the grains are highly fractured and a chemical investigation is needed to be certain. It is found in between two garnetiferous biotite-rich units with equal mineral assemblages. The garnetiferous gneiss (sample 497607) has a mineral assemblage of quartz+plagioclase +biotite+garnet+oxides, but the lower garnet content, and the higher quartz and plagioclase content give the unit a more gneissic texture compared to the texture of the biotite schist. The three units are considered to represent different stages of pre-metamorphic hydrothermal alteration of the host rock, e.g. a volcaniclastic sediment (a tuff) or a tholeiitic basalt. Garde (2007b) argues that the hydrothermal alteration must have taken place prior to the regional deformation, since the unaltered pocket of amphibolite (the cores in the garnetiferous biotite schist) would otherwise have been deformed. This can only be the case if the layer has behaved as a competent layer during the deformation, otherwise the two unaltered cores would probably have formed boudin structures during the deformation. As described in section 5.1.2 competent layers, showing signs of hydrothermal alteration, are undeformed within an amphibolite layer and have boudin structures (see Figure 6). Thus, competent hydrothermally altered layers surviving deformation occur in the area. Some biotite grains in the garnetiferous biotite gneiss show distortion textures, which is a sign of deformation. However, it is not possible to conclude when the distortion was formed because not all the biotite grains show this feature. Hence, from the field, hand specimen and thin section examinations it can not be concluded if the hydrothermal alteration took place prior or after the deformation of the area.

Seven samples have been collected in four sulphide-mineralized layers of which only one is auriferous. The rocks have mineral assemblages of quartz+plagioclase+mica Mg-rich hornblende garnet oxides+sulphides. Plagioclase is the end-member albite with some amount of the anorthite phase seen in the XRD analysis results, where the albite is named “calcian albite”. Biotite is the dominating mica, but sample 497608 contains a small amount of muscovite and no biotite. Sample 497610 is an amphibolite. Samples 497609 and 497611 are garnet amphibolites. Sample 497612 is a biotite gneiss, and sample 497613 is a garnet-biotite gneiss. Sample 497608 represents a quartz vein (~30 cm across) that shows hydrothermal wall rock alteration as albitization and sericitization. These processes are often found in rocks associated with ores (Evans 1993). Sericitization occurs when potassium is introduced into a rock low in this element. With the appearance of secondary potash feldspar sericitization grades into potassic alteration which is very common in porphyry copper deposits, e.g. Bingham Canyon, Utah. In potassic altered rocks the common sulphides are pyrite, molybdenite and chalcopyrite (Evans 1993). Albitization observed in the thin section, and confirmed by a content of 2.11 % Ca compared to 6.17 % Na, is in agreement with the suggestion of hydrothermal alteration being the cause of a positive Eu anomaly seen in the REE pattern (see section 6.1.1).

The supracrustal rocks described and discussed in this thesis show no proof for or against an island arc complex. The samples represent volcanic rocks metamorphosed to amphibolite facies. Several discoveries made by Garde (2005; 2007a,b), such as fragmental amphibolites with volcaniclastic textures, fiamme textures and graded bedding, suggest an island arc setting with explosive volcanism, hence, sub-aqueous or sub-aerial volcanic activity.

6.3.2 Supracrustals from the north-western Qussuk peninsula

The samples collected in the north-western Qussuk area have been metamorphosed to lower granulite facies, hence they do not come under the general definition of a greenstone even if some of them contain hornblende. The two samples containing orthopyroxene (497685) and clinopyroxene (497686) have been discussed above in section 5.1 dealing with metamorphism of the area. While containing up to 25 % orthopyroxene sample 497685 is named a pyroxene-amphibolite due to a hornblende content of ~65 %. Samples 497686 and 497687 are from the same sulphide-mineralized layer, and although clinopyroxene has only been observed in sample 497686 in thin section, it has been identified by XRPD in sample 497687 as well. Thus, they are considered to represent the same leucocratic amphibole-pyroxenite (5 % hornblende and 10% augite-hedenbergite) with sample 497686 representing a siliceous and plagioclase-rich vein within the leucocratic unit (sample 497687). As suggested in section 6.1.1 the positive Eu anomaly occurring in sample 497686 could have been formed by hydrothermal alteration such as albitization. However, in the thin section albitization is hard to determine. The larger and more abundant grains show first-order yellow intereference colour which only occurs for very calcic plagioclase (Nesse 2004). This is in agreement with the XRPD results, where anorthite is the identified plagioclase, as well as a low sodium bulk concentration of the rock (Figure 27). Thus, the positive Eu anomaly is explained solely by the high content of plagioclase of ~30 % in the

sample. Furthermore, a cordierite grain, c. 2 mm in length, is found in sample 497686. Cordierite is an abundant mineral in sample 497689, discussed in detail below, and the cordierite grain occurring in sample 497686 connects the two rock units, but no conclusions can be made on the basis of a single grain.

Orthoamphibole-cordierite gneiss

Sample 497689 is different from to the other rocks collected in the area with a mineral assemblage of anthophyllite+cordierite+quartz+plagioclase+biotite+almandine. Cordierite-anthophyllite rocks are chemically unusual rock types that do not correspond to any common type of igneous, sedimentary or metamorphic rock. Rocks with this mineral assemblage are characterized by enrichment in Mg, Al, and Ti and by moderate to extreme depletion in alkalis and Ca (Schneiderman and Tracy 1991). Anthophyllite is unknown in igneous rocks but occurs in a wide range of rocks of metamorphic and metasomatic origin, the metamorphism reaching amphibolite facies (Yardley 1989). Cordierite is most common in metasediments but does occur in igneous rocks (Deer et al. 1992). The cordierite-anthophyllite assemblage is usually considered to result from the metamorphism of volcaniclastic sediments of basaltic composition with the bulk composition modified by some pre-metamorphic alteration by hydrothermal fluids, especially by seawater (Spear 1993). Alteration by seawater is a well established large scale phenomenon in island arc environments (Robinson et al. 1982). Cordierite-orthoamphibole rocks have been intensely studied due to their common association with massive Fe-Cu-Zn-Pb sulphide deposits (Schneiderman and Tracy 1991).

6.3.3 Garnet composition

Garnets in samples 497605 and 497609 from the central Qussuk peninsula and in sample 497689 from the north-western Qussuk peninsula were analyzed by EMPA. They are all in the pyralspite group although all of the grains contain some amount of the grossular end-member of the ugrandite group. A fairly complete and continuous variation in composition occurs within these two series, but there appears to be a less continuous variation between pyralspite and ugrandite (Deer et al. 1982, 1992). The end-member components have been calculated following Rickwood (1968) and names have been assigned according to the dominant molecule present, which in all cases is almandine, although the percentage of pyrope is high enough and the percentages of the other end-members low enough to justify the name almandine-pyrope in samples 497605 and 497689.

The anomalous garnetiferous biotite schist (sample 497605) is a c. 2 m wide layer with a garnet content of up to 80 %. In the field, two round cores (c. 15 cm in diameter) with no garnet content occurred. From the cores and outwards, a zone with gradational increasing garnet content occurred. The garnet-lacking cores are interpreted to be reminiscent of unreplaced original rock in a layer that was hydrothermally altered prior to metamorphism. The hydrothermal alteration of the layer favoured garnets to be formed during metamorphism. The garnets are almandine-pyropes with an average composition of $Alm_{67}Gro_5Pyr_{27}Sp_1$. The grains are poikiloblastic enclosing biotite and plagioclase and have numerous microscopic quartz and ilmenite inclusions. The almandine composition, along

with the poikiloblastic texture, is evident of a metamorphic garnet resulting from regional metamorphism (Deer et al. 1992).

Garnet analyzed in sample 497609 has a composition of $Alm_{56}Gro_{19}Pyr_{11}Sp_{14}$, hence, having a significant amount of both the spessartine and grossular molecules. The grain is poikiloblastic enclosing the other silicates in the rock and has a homogenous composition. The spessartine molecule can be present in significant amounts in almandine from metamorphic rocks, but it is rarely dominant in such an environment (Deer et al. 1992). Often almandines that contain a considerable amount of the manganese-bearing end-member show chemical zoning, which is another sign of regional metamorphism. The zoning is formed by an antipathetic relationship between Fe and Mn that usually gives a Mn-rich core and Fe-rich margin of the garnet (Deer et al. 1982). However, chemical zoning is not evident in the garnet. The homogenous texture of the grain can be explained by a total re-crystallization of the garnet which is the result of the strong metamorphic effect in the area. From the same area zircons analyzed by Garde (2007a) also show sign of re-crystallization.

The cordierite-anthophyllite bearing rock (sample 497689) from the north-western Qussuk area has a high content of garnet. The garnets observed in the field are up to 10 cm in diameter, however, the garnets in the hand specimen are only up to ~1 cm in diameter. The grains are characteristically poikiloblastic enclosing cordierite, biotite and plagioclase and have quartz and opaque inclusions. The homogenous composition of the garnet is $Alm_{58}Gro_{4}Pyr_{36}Sp_{2}$, thus, it is very similar to that of the garnet in sample 497605. The almandine-pyrope composition and the poikiloblastic texture of the garnet are evident of a metamorphic origin.

Garnet occurs in many of the samples and it is not confined to a particular host rock or mineral association. It is considered to have been formed during the regional metamorphism of the area. From the results of the XRPD analyses, it could be argued that garnet in the sulphide-mineralized layers has the same average composition (spessartine), in which case the garnets would have similar compositions as that of sample 497609 ($Alm_{56}Gro_{19}Pyr_{11}Sp_{14}$). A Rietveld refinement was run on sample 497613 showing a composition with more of the spessartine end-member than of the almandine end-member. The Mn content in this sample is 0.30 w% and actually much higher than in the rest of the samples with weight percentages between 0.08 and 0.17 Mn. Hence, the chemical analysis supports the result from the Rietveld refinement. However, caution must be applied when dealing with the identification of garnet by XRPD results. Garnets show great variations in compositions due to the continuous variation between and within the two garnet series, hence, the composition of the garnets used as the standard XRD patterns may not be representative of garnet in a specific rock. Garnets from different areas seldom have same average compositions and even within one area garnets show varying compositions, such as it is seen in the area described in this thesis, as a result of different host rocks. Furthermore, as Deer et al. (1982) point out, a garnet with a composition corresponding to anyone end-member is rare. In general, XRPD results can be used to either recognize or confirm the occurrence of garnet in a sample, but the compositions of particular garnet grains should be established by the EMPA.

6.3.4 Ore mineralogy

Microscopically, primary sulphides occur mostly as disseminated grains in varying sizes from fine to coarse grained along silicate grain boundaries and as inclusions in silicate grains. The sulphides also occur as thin vein and fracture fillings. They are anhedral, often rounded and very rarely euhedral grains associated with all the silicates in the rocks. The most dominating sulphide is pyrrhotite and the second-most dominating is chalcopyrite, both occurring as the largest sulphide grains (up to 5 mm). Several grains with both pyrrhotite and chalcopyrite occur in many of the sulphide-rich samples and are interpreted to represent the primary sulphide content. Pyrite is common in some samples and often exhibits subhedral to euhedral forms. Microscopic grains of sphalerite at the edges of pyrrhotite occur (sample 497609). Several round microscopic grains within silicate grains occur and are considered to be possibly arsenopyrite. Several sulphide grains show evidence of paragenesis with the silicates, e.g. in form of euhedral biotite within pyrrhotite (sample 497611), and some larger sulphide grains contain inclusions of silicates. Secondary sulphides formed during weathering are marcasite and covellite, which are discussed in detail in section 6.3.5. In the auriferous sample (497686) from the north-western Qussuk peninsula semi-massive pyrrhotite and chalcopyrite occurs in the hand specimen (Figure 29).

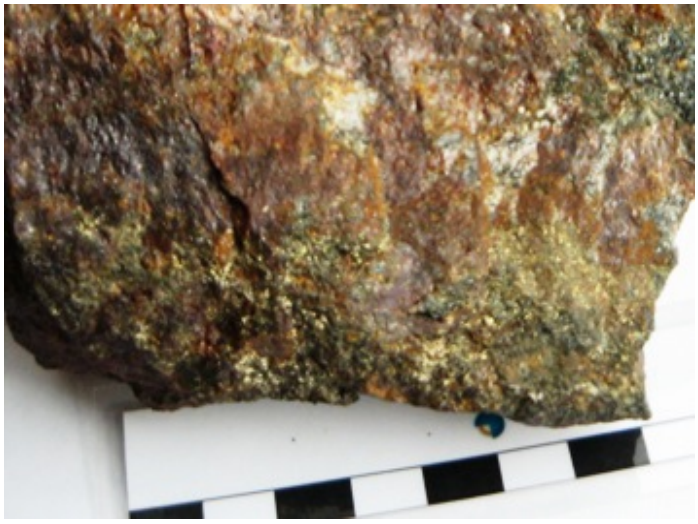

Figure 29. *Semi-massive sulphides (pyrrhotite and chalcopyrite) in sample 497686 from the north-western Qussuk peninsula.*

The Fe-Ni sulphide pentlandite is identified by XRD in sample 497687 from the north-western Qussuk peninsula. Other sulphides identified both by XRD and in the thin section are pyrite, pyrrhotite and marcasite. Pentlandite is often associated with pyrrhotite as the result of exsolution occurring after magmatic segregation. At higher temperature and pressure conditions, the chemical constituents of the two minerals are compatible, but with a decrease in temperature and pressure, the two chemistries become incompatible and they separate into two different minerals. Pentlandite and pyrrhotite have similar properties, e.g. colour, streak, hence the two minerals are difficult to differentiate when pyrrhotite is in a massive form (all from “The mineral pentlandite”, 2007, 13 May). However, since pentlandite has not been identified in the thin section there is no base to conclude on the presence or genesis of the mineral.

Oxides occurring in the rocks show both primary and secondary textures. The oxides are dominated by ilmenite and magnetite. Hematite occurs in one sample (497689). In most samples with an oxide content anhedral to subhedral (tabular), fine to very fine grained ilmenite occurs as disseminated grains, as inclusions in silicates (in particular garnet) and some of the grains cut silicate grain boundaries. It also occurs as fillings of fractures in garnet grains. Ilmenite occurs both as primary and as secondary grains, the latter have been formed during metamorphism of the rocks. Secondary magnetite occurs together with ilmenite in association with goethite. Magnetite is anhedral and fine grained. Primary magnetite showing ilmenite lamellae (titanomagnetite) occurs in samples from the northwestern Qussuk peninsula. The lamellae of ilmenite in magnetite are formed by an oxidation-exsolution process as magnetite-ulvöspinel cool from the temperatures of initial crystallization or the maximum temperature of metamorphic re-crystallization. Oxidation of the magnetite-ulvöspinel will happen if cooling goes on along a buffer curve or in the presence of a fluid of constant composition, and ilmenite lamellae will be formed (Craig and Vaughan 1994).

6.3.5 Weathering

When meteoric (oxygenated) water reacts with sulphide-bearing rocks an encrusting mass, a so-called gossan, enriched in supergene minerals may develop on or just below the surface (Figure 30). Oxidation of metals by water reacting with sulphides forms oxides, hydroxides, carbonates and sulphates (Nesse 2000). By field observations alone, it is evident that many of the sulphide-rich layers in the research area are strongly weathered. This is apparent from the characteristic yellow-brown to reddish colour of the alteration product. The hydroxide goethite is formed as iron sulphides decompose during surface or near-surface oxidation to yield sulphuric acid and soluble ferrous sulphate. Base-metal sulphides are dissolved by the acid, and the ferrous sulphate oxidizes to bring about mixed iron oxides (Craig and Vaughan 1994). Goethite occurs in several of the sample specimens filling out veins and fractures, replacing iron-rich sulphide minerals partly, hence leaving variable amounts of residual sulphides, or creating pseudomorphs after sulphides commonly preserving the primary grain shapes (Craig and Vaughan 1994). Goethite sometimes forms the characteristic boxworks texture (also called gossan) which is observed in sample 497610.

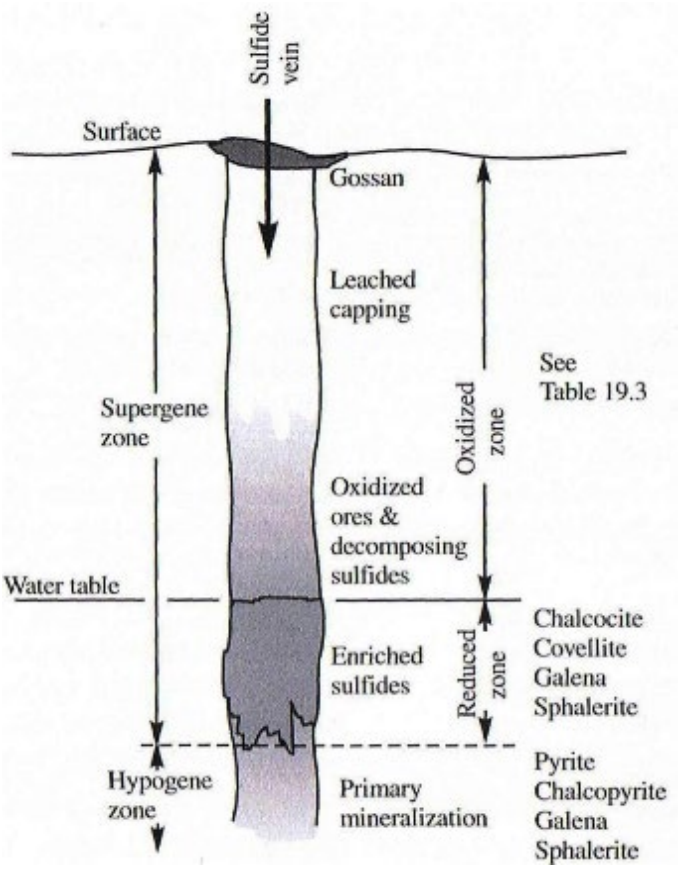

Figure 30. *Supergene enrichment from meteoric water percolating down through a sulphide-bearing rock. In the upper part of the oxidized zone iron oxides and hydroxides replacing iron-rich sulphides form a gossan. From Nesse 2000.*

Another sign of weathering of the rock specimens is where marcasite replaces pyrrhotite forming “birds-eye” textures. The replacement of pyrrhotite by marcasite is a sign of the deepest level of weathering above the water table and occurs in several of the samples, e.g. 497686 and 497610. It is a chemical alteration, termed a topotactic transformation, where internal atomic displacements of Fe occur. Half of the Fe in pyrrhotite, $Fe_{1-x}S$, is washed out and disulphide bonds replace the Fe sites forming FeS_2, the chemical formula for pyrite and marcasite. Pyrrhotite has a pseudohexagonal crystal form, and marcasite is orthorhombic giving three possible ways of marcasite to lie on top of pyrrhotite but marcasite always has one and the same axis in common with pyrrhotite. This means that less energy is required for pyrrhotite to be replaced by marcasite than by pyrite, which is isometric. The replacement of pyrrhotite by pyrite does occur but under higher temperature (all from Makovicky 2006; Makovicky pers. comm.).

Covellite is a typical secondary mineral formed by oxidation of other sulphides. It most commonly occurs as pseudomorphic replacements after chalcopyrite, and rarely pyrite, enargite, chalcocite and other sulphides (Ramdohr 1969; Deer et al. 1992). Replacement may selectively remove one cation while leaving another and replacement of chalcopyrite by covellite occurs (Craig and Vaughan 1994). Covellite occurs in several of the samples collected in the central Qussuk peninsula as irregular replacement without any relation to the forms of chalcopyrite.

Due to the intense weathering of the sulphide-mineralized layers the original sulphide mineral composition can be difficult to determine. Also, since a high percentage (up to 10 %) of sulphide grains are replaced wholly or partly by goethite the initial sulphide content has been higher in the rocks. Thus, the ore potential insights resulting from determining the sulphidation states of gold mineralisation may be elusive to determine from field examination of rocks, and hence, willingness to drill is crucial (Simmons et al. 2005).

6.4 Gold Mineralisation

Proof of gold in the supracrustal rocks comes from geochemical analyses only. The highest gold concentration is found in the central Qussuk peninsula. It occurs in a thin quartz vein with signs of albitization and sericitization adjacent to amphibolites also containing varying concentrations of Au and with varying content of quartz veinlets and garnet. The gold is found in samples 497608, 497609, 497610 and 497611 with 8160, 1540, 2470 and 819 ppb Au, respectively. The samples are from one sulphide-mineralized layer in the central Qussuk peninsula, which is described in greater detail in Appendix A as well as in the discussion above. The sulphides dominate the auriferous rocks and carry disseminated chalcopyrite and pyrrhotite with minor pyrite, marcasite, covellite, sphalerite and arsenopyrite (?). However, in the samples with the two highest gold concentrations (497608 and 497610) a significant amount of pyrite occurs as euhedral to subhedral grains <1 mm in length.
In the north-western Qussuk area, one auriferous sample (497686) is characterized by high silica content and semi-massive sulphides apparent in the hand specimen. The dominating sulphides are pyrrhotite associated with chalcopyrite and pyrite, and significant amount of marcasite formed during weathering of the rock. Pyrrhotite and chalcopyrite are fine to coarse grained. The gangue mineral is both coarsely crystalline and fine grained recrystallized quartz and coarse grained plagioclase.

Although the definition of greenstones is accepted world-wide, it can generally be difficult to classify gold deposits in greenstone belts because of the diversity of the deposits and the different degrees of metamorphism. However, many deposits have some common characteristics and are classified on the basis of those. The hydrothermal alteration and associated gold mineralisation in the Qussuk area is proposed by Garde et al. (2007) to be synvolcanic and epithermal in origin. In the following, both the stratiform exhalative volcanic-associated sulphide gold deposit and the epithermal gold model will be discussed, as well as remobilization of gold during orogenesis.

6.4.1 Gold deposit models

Stratiform exhalative sulphide deposits
Volcanic-associated massive sulphide gold deposits are a subtype of stratiform exhalative sulphide deposits deposited directly on the seafloor or in the immediate subseafloor (Figure 31). Gold is the primary product with copper, zinc, silver and lead of less economic significance. Per definition the gold in ppm exceeds the associated combined Cu, Zn and Pb in weight per cent (Dubé et al. 2007). The gold concentrations are typically of 1 to 2 ppm, but

as high as 10-15 ppm. Such deposits are typically hosted in rocks of volcanic affinity formed in tectonic settings of island arcs, rifted arcs, or back-arc basins. The host sequences characteristically comprise a mafic component in the form of basalt, andesite, or amphibolite and a felsic component in the form of tuffs and volcanic breccias. Although the name refers to ore bodies of massive character, many of the copper-gold deposits consist largely of disseminated and stockwork-like vein systems and, hence, are strictly speaking not massive sulphide ores. The distribution, proportion and composition of ore types display considerable variation amongst the deposits. The dominating sulphides are massive pyrite, pyrrhotite and chalcopyrite associated with sphalerite, galena, arsenopyrite, magnetite and others. Tellurides might be present too. Wall rock alteration is a common feature, and pyritic, quartz-sericite schists are the most common hosts. The deposits typically occur together with conventional base metal massive sulphide deposits and share many of their geological characteristics (all from Poulsen and Hannington 1995).
An example of auriferous massive sulphide deposits is the Joutel district which is distributed in Archaean greenstone belts within the Superior Province, Canada, (Dubé et al. 2007).

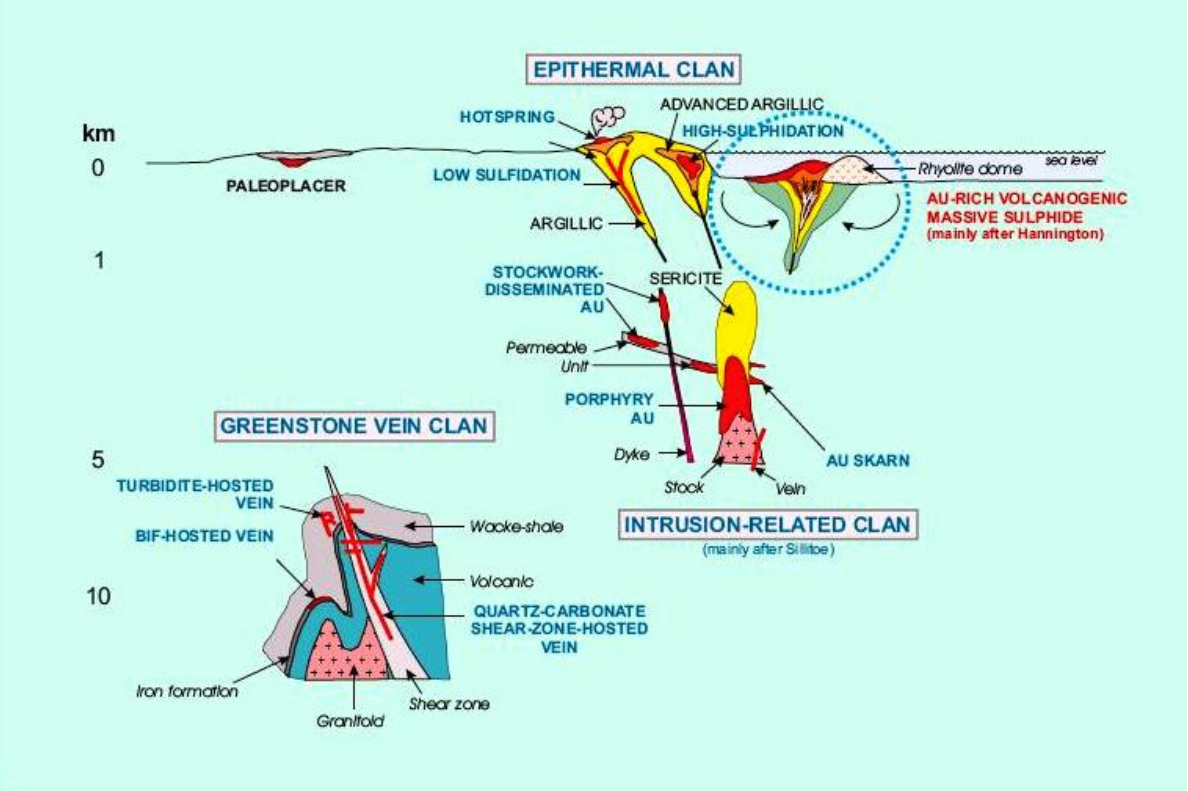

Figure 31. *Schematic illustration of the various types of gold deposits shown at their inferred crustal levels of formation. The auriferous volcanogenic massive sulphide deposit is deposited on the seafloor or in the immediate subseafloor. High-sulphidation epithermal deposits are associated with a magmatic-hydrothermal system dominated by acid hydrothermal fluids. From Dubé et al. 2007.*

Epithermal gold deposits

Epithermal ore deposits are associated with a magmatic-hydrothermal system and formed at temperatures < C and depths <1.5 km (Figure 31). Such hydrothermal systems generally develop in association with calc-alkaline magmatism, in volcanic arcs at convergent plate margins and in intra-arc, back-arc and postcollisional rift settings (Simmons et al. 2005).

Epithermal ore deposits are divided into two main types based on their alteration mineralogy, where the high-sulphidation type is typical of acidic springs near volcanoes and the low-sulphidation type is found in geothermal systems (Figure 32). Here, focus is on the high-sulphidation ore deposit type in which the host rocks are characterized by extensive leaching by fluids with a pH <2 and an O- and H-isotope composition similar to that of a magmatic vapour mixed with meteoric water. The fluids involved have isotopic composition similar to high-temperature volcanic vapours. The ores are characterized by porous silica residues formed by the extensive leaching, and these residues may subsequently host Au-bearing Cu- and Fe-sulphides. The mineralogical characteristics of the high-sulphidation ore deposits have similar characteristics to that of the advanced argillic zone of alteration associated with porphyry Cu deposits. Commonly, there is a close spatial relationship between high-sulphidation epithermal Cu-Au deposits and porphyry Cu deposits, the latter are associated with intrusions and characterized by involvement of magmatic fluids (all from Hedenquist and Lowenstern 1994). The advanced argillic alteration zone is characterized by dickite, kaolinite, pyrophyllite and quartz with sericite usually present and frequently alunite, pyrite, tourmaline, topaz and zunyite (Evans 1993). The main gangue minerals are both coarsely crystalline quartz and alunite. The sulphides occurring in this deposit type are pyrite in variable amounts, Cu-sulphides and sulfosalts with enargite (Cu_3AsS_4) as the dominating one indicating a high sulphidation state (Simmons et al. 2005).
Given the relative shallow depth of formation, epithermal gold deposits may have poor preservation potential in the geologic record. Thus, most of the known epithermal deposits are Tertiary or younger. However, Precambrian examples are reported for e.g. Canada, but the known very ancient epithermal deposits are small (Simmons et al. 2005). An example of an Archaean epithermal gold deposit is the Archaean Racetrack Au-Ag deposit near Kalgoorlie, W. Australia (Gebre-Mariam et al. 1993).

6.4.2 The Qussuk gold mineralisation

The gold mineralisation in the Qussuk area has a distinct Au-Cu association which correlates well with both the volcanic-associated massive sulphide gold deposit and the epithermal gold deposit models. Additionally, the host rocks for the ores in the two models are of volcanic affinity considered to have formed in arc environments, e.g. island arcs, rifted arcs and back-arc basins at convergent plate margins. The supracrustal rocks in the Qussuk area are of volcanic affinity considered to represent a relict island arc complex.
In the epithermal system the Cu-As-sulphosalt enargite is the dominating Cu-sulphide (Simmons et al. 2005). The Cu-sulphide identified in the supracrustal rocks is chalcopyrite which is considered to be primary together with pyrrhotite. Even under higher temperature metamorphism (upper amphibolite and lower granulite facies), the Cu-As-sulphosalt enargite would re-crystallize to tennantite ($(Cu,Fe)_{12}As_4S_{13}$) (McDonald 1967). Tennantite has not been identified in any of the supracrustal rocks of the area. Aditionally, the Qussuk gold differs from the epithermal model by having pyrrhotite rather than pyrite as the dominating sulphide. This suggests a higher temperature (> 400°C) formation of the ores. The main gangue mineral and host rocks of the Qussuk gold correlates with the epithermal deposit model.
One of the more important points that the Qussuk gold possibly has formed in a volcanic-associated massive sulphide gold deposit is the fact that gold is the main commodity com-

pared to the other base metals since the gold in ppm exceed the combined Cu, Zn and Pb in weight per cent in the samples with the highest gold concentrations (8 ppm Au vs. 0.5 % Cu+Zn+Pb in sample 497608 from the central Qussuk peninsula and 5 ppm Au vs. 0.1 % Cu+Zn+Pb in sample 497686 from north-western Qussuk area). Additionally, pyrrhotite is one of the major ore minerals in the auriferous massive sulphide deposits together with pyrite and chalcopyrite, which is consistent with the ore mineral assemblage of the supracrustal rocks. Furthermore, in the north-western Qussuk area an anthophyllite-cordierite gneiss occurs, which is commonly associated with massive Fe-Cu-Zn-Pb sulphide deposits (Schneiderman and Tracy 1991).
Tellurium is often present in both the gold deposits described above, but the lack of tellurium in the two auriferous samples (497608 with 1.1 ppm Te and 497686 with 1.2 ppm Te) in the Qussuk area can be explained by pyrrhotite in general being the dominating sulphide in the supracrustal rocks. The occurrence of pyrrhotite correlates with the typical absence of tellurides in ore zones reflecting the limited solubility of tellurium in reduced ore fluids at sulphur fugacities above the pyrrhotite-pyrite buffer (Goldfarb et al. 2005).

It is generally accepted that ore deposits of the Precambrian shields, particularly the Late Archaean greenstone belts, are classified as epigenetic gold deposits in metamorphic terranes (Goldfarb et al. 2005). These gold deposits are considered to be of orogenic origin formed in the forearc region of a convergent continental margin. Most of the orogenic gold deposits formed in the late stages of the orogenic process but commonly postdates the metamorphism, typically at greenschist to lower amphibolite facies, of the host rocks. However, there is little doubt that these ores have been formed by deposition from hydrothermal solutions into open fissure and fracture systems, and it is thought that the gold may have been derived from the enclosing rocks and concentrated by circulating fluids during metamorphism (Craig and Vaughan 1994). This general opinion makes room for the suggestion that both epithermal gold deposits and stratiform exhalative auriferous massive sulphide deposits, which are formed prior to metamorphism and deformation of an area, could have been remobilized into an orogenic gold deposit. This would explain the Au-Cu association generally not seen in orogenic gold deposits, which is typically enriched in trace elements including Ag, As, Au, B, Bi, Hg, Sb, Te and W. Additionally, the hydrothermal influence on the gold-bearing rocks, or in any case the sample with the highest gold concentration, is confirmed by the strong positive Eu anomaly and the albitization and sericitization of the rock.

Many of the data represented favours the stratiform exhalative volcanic-associated massive sulphide gold deposit model compared with the epithermal gold deposit model. However, the original features of these ore deposit types have presumably changed through metamorphism and deformation which makes it difficult to establish the origin of the gold mineralisation based on the data presented in this thesis. Nevertheless, it is evident that the gold mineralisation is not an epigenetic orogenic deposit. The paragenesis of the mineral assemblages implies that the sulphides were formed prior or contemporaneous with metamorphism and not postdating the metamorphic event as is typical of the orogenic gold deposits. It is assumed that the gold formed syngenetic with the sulphides. The distinct Au-Cu association is also not comparable to an orogenic origin of the gold.
It is suggested that the gold was formed syngenetic in either an epithermal system or (more likely) as a volcanic-associated massive sulphide gold deposit. A following deformation of

the area remobilized the gold and sulphides into open fissure and fracture systems forming the veins dominated by gold and quartz in highly deformed and metamorphosed volcanic rocks as is typical of orogenic gold deposits according to Robert (1995). This suggestion correlates to some extend with Garde's proposal (2007a) as it is shown in Figure 32, where Garde has presented a possible deformation scheme of the Akia terrane including the relict island arc system in the Qussuk area. However, the origin of the gold mineralisation could be either epithermal or stratiform exhalative, since both types are formed in volcanic arc systems.

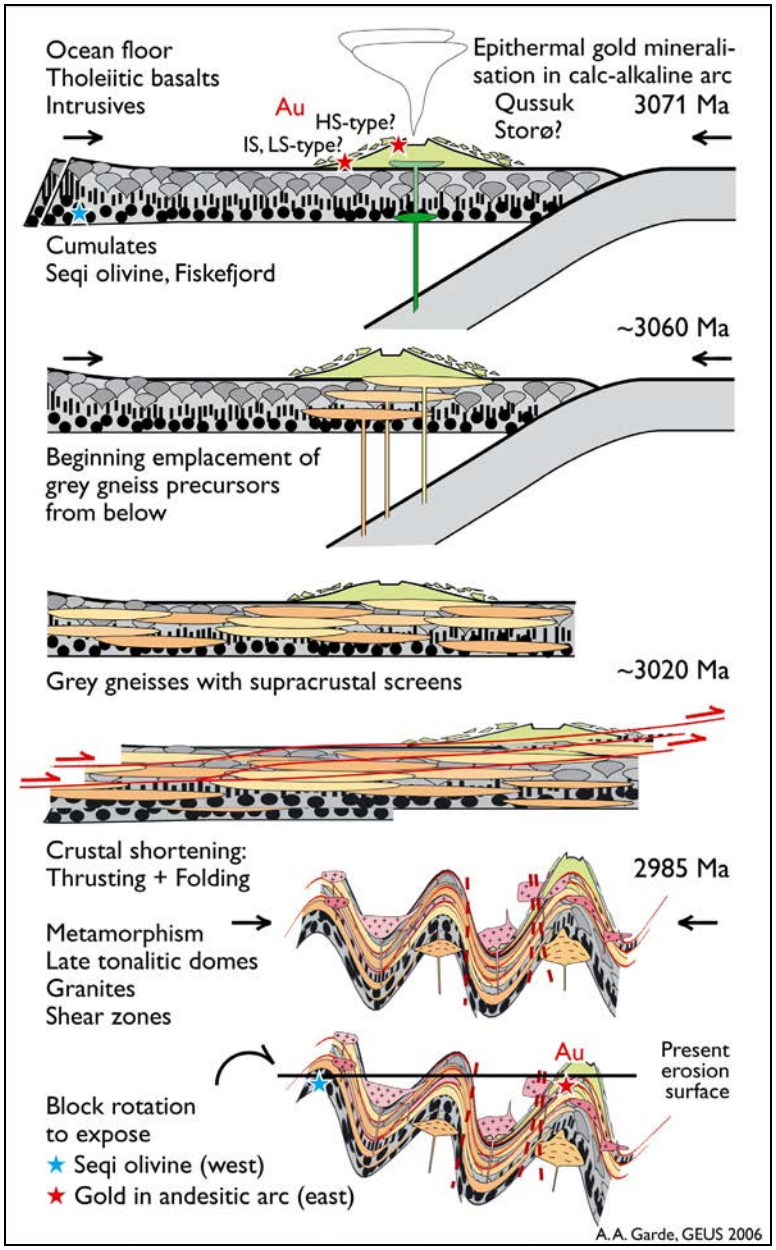

Figure 32. *Schematic illustration of the prinicipal stages in the magmatic and tectonic accretion of the Akia terrane as proposed by Garde (2007a). The gold mineralisation can be either epithermal or exhalative. From Garde (2007a).*

7. CONCLUSIONS

1) The Qussuk peninsula represents a relict island arc complex of Mesoarchaean age. The supracrustal rocks of the central part are represented by mafic and leucocratic amphibolites that can be characterized as greenstones due to their amphibole content. The rocks have been exposed to hydrothermal alteration in varying degrees, some possibly prior to the deformation of the area. The general mineral assemblage is quartz+plagioclase+hornblende+biotite ± garnet ± sulphides ± oxides. According to the geochemical data the rocks comprise two main components: (1) a mafic component of low-K tholeiitic affinity, and (2) a leucocratic component of basaltic to andesitic affinity. The geochemical data gives mixed results as to whether the leucocratic amphibolites are of basaltic or andesitic affinity. The LREE enriched REE patterns with relatively flat HREE as well as the N-MORB normalized spider diagrams suggest an andesitic origin, but the high nickel, cobalt and chromium concentrations along with the inconsistent Ni/Co and V/Ni ratios contradict the suggestion made by Garde (2007a) that the amphibolites are all of andesitic affinity. According to the data published by e.g. Peccerillo and Taylor (1976) and Taylor et al. (1969b) only four of the rocks presented in this thesis are of andesitic affinity

2) The supracrustal rocks of the north-western Qussuk peninsula are represented by volcanic or volcanoclastic pyroxene- and amphibole-bearing rocks and are not classified as greenstones, neither by their geochemical characteristics nor by their mineralogical assemblages. The rocks show very varied mineral assemblages and geochemical characteristics. An orthoamphibole-coriderite gneiss different from the other rocks in the area represents a volcaniclastic sediment exposed to metasomatism prior to metamorphism. This type of rock implies an association with massive Fe-Cu-Zn-Pb sulphide deposits.

3) The central area of the Qussuk peninsula has undergone metamorphism to amphibolite facies which is in accordance with the general opinion. On the contrary, mineralogical evidence such as poikiloblastic orthopyroxene porphyroblasts suggests that the northwestern part of the Qussuk peninsula has undergone granulite facies metamorphism and partly retrogressive metamorphism to amphibolite facies. This is contradictive to the proposal made by Garde (2000; 2007a) that the whole area North and East of the Qussuk bay (hence, including the Qussuk peninsula) has undergone metamorphism to amphibolite facies only.
Many of the supracrustal rocks have varying garnet content. The garnets analyzed display typical metamorphic compositions.

4) The dominating sulphides are pyrrhotite and chalcopyrite, and significant amounts of pyrite occur in the auriferous quartz veins. Sphalerite occurs in several of the rocks and pentlandite has been identified by XRD in one. Secondary marcasite in significant amounts and covellite replace the iron-sulphides, namely pyrrhotite and chalcopyrite. The sulphides occur as disseminated to semi-massive grains in paragenensis with the silicates. Intense weathering of the sulphide-mineralized layers has formed excessive goethite which obstructs the determination of the original sulphide mineral composition and content. The oxides in the rocks are mainly disseminated ilmenite and magnetite occurring both as primary

and secondary grains. Hematite occurs in one sample.

5) The two rocks (497608 and 497686) with the highest gold concentrations are in many ways similar. They show (i) Au-Cu association with gold as the main commodity over base metals (Cu, Zn and Pb), (ii) quartz as the gangue mineral, (iii) pyrrhotite, chalcopyrite and pyrite as the dominating sulphides, (iv) strong positive Eu anomalies and (v) intense weathering in the form of excessive goethite content. However, a few dissimilarities occur as well: (a) sample 497608 shows sign of hydrothermal alteration such as albitization and sericitization, and (b) semi-massive sulphides occur in sample 497686.

6) The origin of the gold mineralisation in the Qussuk area can not be concluded from the data presented in this thesis. Nevertheless, a syngenetic origin of the gold and the volcanic island arc with a following remobilization of the gold into quartz veins formed in fissures and fractures during deformation and/or metamorphism is suggested. The Au-Cu association disproves the general idea that gold occurrences in Late Archaean greenstone belts are of epigenetic orogenic origin and points towards a volcanic-associated massive sulphide gold deposit or an epithermal gold deposit. The majority of the data correlate with the former, but the original features of the ore deposit have presumably changed during the deformation and the moderate to high grade metamorphism of the area.

8. ACKNOWLEDGEMENT

I appreciate the advice and feedback of my advisors Senior Research Scientist, Ph.D. Henrik Stendal (GEUS) who also made this report a reality, and Professor Emil Makovicky (Geological Institute, University of Copenhagen). I thank GEUS for the opportunity to be part of the field work 2005.

Many people have been involved at different levels: Adam Garde (GEUS), Jens Konnerup (Geocenter), Lars Olsen (Geocenter) and Gorm Thøgersen; thank you for helpful guidance in the field as well as with data results and helpful discussions along the way. Helene Almind (Geocenter), Hanne Lamberts (GEUS), Peter Venslev (Geocenter), Berit Wenzell (Geocenter) and Jørgen Kystol (GEUS); I appreciate your guidance, help, assistance and the great times in the different laboratories. Thank you all.

9. REFERENCES CITED

Alle Nyheder; Meddelese nr. **2/2006** (2006, 22 February) Positive resultater af guldefterforskning ved Qussuk. Retrieved 5 December 2007 from http://nunaminerals.com/database.asp?lang=dk&num=346&page=arkiv_nyhed&menu=6

Alle Nyheder; Meddelese nr. **35/2007** (2006, 26 July) Boremål for kobber og guld lokaliseret ved Qussuk. Retrieved 5 December 2007 from http://nunaminerals.com/database.asp?lang=dk&num=369&page=arkiv_nyhed&menu=6

Anders, E. and Grevesse, N. 1988: Abundances of the elements: Meteoritic and solar. Geochemica et Cosmochemica Acta **53**,197-214.

Andreasen, B. 2007: Mineralogical and geochemical investigations of gold-bearing Mesoarchaean supracrustal rocks from Qussuk area, West Greenland, 106 pp. Unpublished M.Sc. thesis, University of Copenhagen.

Appel, P.W.U.; Bliss, I.C.; Coller, D.W.; Grahl-Madsen, L. and Petersen, J.S. 2000: Recent gold discoveries in Archaean rocks of central West Greenland. Institution of Mining and Metallurgy, Trnasactions, Section B: Applied Earth Science **109**, 34-41.

Appel, P.W.U., Garde, A.A., Jørgensen, M., Moberg, E.D., Rasmussen, T.M., Schjødt, F. and Steenfelt, A. 2003: Preliminary evaluation of the economic potential of the greenstone belts in the Nuuk region. General geology and evaluation of compiled geophysical, geochemical and ore geological data. Danmarks og Grønlands Geologiske Undersøgelse Rapport **2003/94,** 147 pp.

Bau, M. 1991: Rare-earth element mobility during hydrothermal and metamorphic fluid-rock interaction and the significance of the oxidation state of europium. Chemical Geology **93**, 219-230.

Berthelsen, A. 1960: Structural studies on the pre-Cambrian of western Greenland. II. Geology of Tovqussap nunâ. Bulletin Grønlands geologiske Undersøgelse **25**, 235 pp.

Craig, J.R. and Vaughan, D.J. 1994: Ore microscopy & ore petrography, 434 pp.

Crowley, J.L. 2002: Testing the model of late Archaean terrane accretion in the southern West Greenland: a comparison of the timing of geological events across the Qarliit nunaat fault, Buksefjorden region. Precambrian Research **116**, 57-79.

Deer, W.A.; Howie, R.A. and Zussman, J. 1982: Rock-forming Minerals Orthosilicates, 467-698.

Deer, W.A.; Howie, R.A. and Zussman, J. 1992: An Introduction to the Rock-Forming Minerals. 2nd edition, 696 pp.

Dubé, B.; Gosselin, P.; Hannington, M. and Galley, A. 2007: Gold-rich Volcanogenic Massive Sulphide Deposits. Pp. 14. Retrieved 17 May 2007 from http://gsc.nrcan.gc.ca/mindep/synth_dep/gold/vms/pdf/deposit_synthesis.gold_vms.dube.pdf

Evans, A.M. 1993: Ore Geology and Industrial Minerals. An Introduction, 389 pp.

Escher, J.C. and Pulvertaft, T.C.R. 1995: Geological map of Greenland, 1:2 500 000. Copenhagen: Geological Survey of Greenland.

Frei, R., Rosing, M.T., Waight, T.E. and Ulfbeck, D.G. 2002: Hydrothermal-metasomatic and tectono-metamorphic processes in the Isua supracrustal belt (West Greenland): A

multi-isotopic investigation of their effects on the Earth's oldest oceanic crustal sequence. Geochimica et Cosmochimica Acta **66**, 467-286.

Friend, C.R.L. and Nutman, A.P. 2005: New pieces to the Archaean terrane jigsaw puzzle in the Nuuk region, southern West Greenland: steps in transforming a simple insight into a complex regional tectonothermal model. Journal of the Geological Society, London **162**, 147-162.

Garde, A.A.; Larsen, O. and Nutman, A.P. 1986: Dating of late Archaean crustal mobilisation north of Qugssuk, Godthåbsfjord, southern West Greenland. Rapport Grønlands Geologiske Undersøgelse **128**, 23-36.

Garde, A.A. 1989: Geological map of Greenland, 1:100 000, Fiskefjord 64 V.1 Nord. Copenhagen: Geological Survey of Greenland.

Garde, A.A. 1997: Accretion and evolution of an Archaean high-grade grey gneiss-amphibolite complex: the Fiskefjord area, southern West Greenland. Geology of Greenland Survey Bulletin **177**, 114 pp.

Garde, A.A. 2007a: A mid-Archaean island arc complex in the eastern Akia terrane, Godthåbsfjord, southern West Greenland. Journal of the Geological Society, London **164**, 565-579.

Garde, A.A. 2007b: A relict island arc complex with synvolcanic epithermal alteration in western Godthåbsfjord, southern West Greenland: field work in 2006 at Qussuk and Bjørneøen. In: Characterisation of selected geological environments. Danmarks og Grønlands Geologiske Undersøgelse Rapport **2007/20**, 13-40.

Garde, A.A.; Friend, C.R.L.; Nutman, A.P. and Marker, M. 2000: Rapid maturation and stabilisation of middle Archaean continental crust: the Akia terrane, southern West Greenland. Bulletin of the Geological Society, Denmark **47**, 1-27.

Garde, A.A., Stendal, H. & Stensgaard, B.M. 2007: Pre-metamorphic hydrothermal alteration with gold in a mid-Archaean island arc, Godthåbsfjord, West Greenland. Geological Survey of Denmark and Greenland Bulletin **13**, 37-40.

Gebre-Mariam, M.; Groves, D.I.; McNaughton, N.J.; Mikucki, E.J. and Vearncombe, J.R. 1993: Archaean Au-Ag mineralization at Racetrack, near Kalgoorlie, Western Australia: a high crustal-level expression of the Archaean composite lode-gold system. Mineralium Deposita **28**, 375-387.

Goldfarb, R.J.; Baker, T.; Dubé, B.; Groves, D.I.; Hart, C.J.R. and Gosselin, P. 2005: Distribution, Character, and Genesis of Gold Deposits in Metamorphic Terranes. Economic Geology, One Hundredth Anniversary Volume**1905-2005**, 407-450.

Hedenquist, J.W. and Lowenstern, J.B. 1994: The role of magmas in the formation of hydrothermal ore deposits. Nature (London) **370**, 519-527.

Hess, P.C. 1989: Origins of Igneous Rocks. Chp. **10**. “Island-Arc Volcanism”, 146-166.

Hofmann, A.W. 1988: Chemical differentiation of the Earth: the relationships between mantle, continental crust, and oceanic crust. Earth and Planetary Science Letters **90**, 297-314.

Hollis, J.A.; van Gool, J.A.M.; Steenfelt, A. and Garde, A.A. 2004: Greenstone belts in the central Godthåbsfjord region, southern West Greenland, Preliminary results from field work in 2004. Danmarks og Grønlands Geologiske Undersøgelse Rapport **2004/110**, 110 pp.

Hollis, J.A. 2005: Greenstone belts in the central Godthåbsfjord region, southern West Greenland, Geochemistry, geochronology and petrography arising from 2004 field work, and digital map data. Danmarks og Grønlands Geologiske Undersøgelse Rapport **2005/42**, 213 pp.

Hollis, J.A.; Schmid, S.; Stendal, H.; van Gool, J.A.M. and Weng, W.L. 2006: Supracrustal belts in Godthåbsfjord region, southern West Greenland. Progress report on 2005 field work: geological mapping, regional hydrothermal alteration and tectonic sections. Danmarks og Grønlands Geologiske Undersøgelse Rapport **2006/7**, 171 pp.

Juul-Pedersen, A., Frei, R., Appel, P.W.U., Persson, M.F. & Konnerup-Madsen, J. 2007: A shear zone related greenstone belt hosted gold mineralization in the Archean of West Greenland. A petrographic and combined Pb-Pb and Rb-Sr geochronological study. Ore Geology Reviews **32**, 20-36.

Klinkhammer, G.P.; Elderfield, H.; Edmond, J.M. and Mitra, A. 1994: Geochemical implicatiosn of rare earth element patterns in hydrothermal fluids from mid-ocean ridges. Geochimica et Cosmochimica Acta **58**, 5105-5113.

Knudsen, C., Van Gool, J.A.M., Østergaard, C., Hollis, J.A., Rink-Jørgensen, M., Persson, M. & Szilas, K. 2007: Gold-hosting supracrustal rocks on Storø, southern West Greenland: lithologies and geological environment. Geological Survey of Denmark and Greenland Bulletin **13**, 41-44.

Lagache, M. and Dujon, S.C. 1987: Distribution of strontium between plagioclases and 1 molar aqueous chloride solutions at 600° at 1.5 kbar and 750°C at 2 kbar. Bulletin of Mineralogy **110**, 551-561.

Lottermoser, B.G. 1989: Rare earth element study of exhalites within the Willyama Supergroup, Broken Hill Block, Australia. Mineralium Deposita **24**, 92-99.

Makovicky, E. 2006: Crystal Structures of Sulfides and other Chalcogenides. In: Sulfide mineralogy and geochemistry. Reviews in Mineralogy and Geochemistry.

Mann, A.C. 1983: Trace Element Geochemistry of High Alumina Basalt–Andesite–Dacite–Rhyodacite Lavas of the Main Volcanic Series of Santorini Volcano, Greece. Contributions in Mineralogy and Petrology **84**, 43-57.

McDonald, J.A. 1967: Metamorphism and its Effects on Sulphide Assemblages. Mineralium deposita **2**, 200-220.

McGregor, V.R.; Friend C.R.L. and Nutman, A.P. 1991: The late Archaean mobile belt through Godthåbsfjord, southern West Greenalnd: a continent-continent collision zone? Bulletin of the Geological Society, Denmark **39**, 179-197.

Nesse, W.D. 2000: Introduction to Mineralogy. Chp.**19** “Sulfides and Related Minerals”, 378-396.

Nesse, W.D. 2004: Introduction to Optical Mineralogy. Chp. **10** “Framework Silicates”, 128-163.

Parlak, O.; Höck, V.; Kozlu, H. and Delaloye, M. 2004: Oceanic crust generation in an island arc tectonic setting, SE Anatolian orogenic belt (Turkey). Geological Magazine **141**, 583-603.

Peccerillo, A. and Taylor, S.R. 1976: Geochemistry of upper cretaceous volcanic rocks from the Pontic chain, northern Turkey. Bulletin of Volcanology **39**, 557-569.

Phinney, W.C. and Morrison, D.A. 1990: Partition coefficients for calcic plagioclase: Implications for Archaean anorthosites. Geochemica et Cosmochemica Acta, **54**, pp. 1639-1654.

Polat, A., Hofmann, A.W. and Rosing, M.T. 2002: Boninite-like volcanic rocks in the 3.7-3.8 Ga Isua greenstone belt, West Greenland: geochemical evidence for intra-oceanic subduction zone processes in the early Earth. Chemical geology **184**, 231-254.

Polat, A., Appel, P.W.U., Frei, R., Pan, Y., Dilek, Y., Ordonez-Calderon, J.C., fryer, B., Hollis, J.A. and Raith, J.G. 2007: Field and geochemical characteristics of the Mesoarchean (~3075 Ma) Ivisaartoq greenstone belt, southern West Greenland: Evidence for

seafloor hydrothermal alteration in supra-subduction oceanic crust. Gondwana Research **11**, 69-91.

Poulsen, K.H. & Hannington, M.D. 1996: Volcanic-associated massive sulphide gold. In: Eckstrand, O.R., Sinclair, R.V. & Thorpe, R.I. (eds): Geology of Canadian mineral deposit types. Geology of Canada **8**, 183-196. Ottawa: Geological Survey of Canada.

Ramdohr, P. 1969: Covellite. In: The ore minerals and their intergrowths, 665-672.

Riciputi, L.R.; Valley, J.W. and McGregor, V.R. 1990: Conditions of Archaean granulite metamorphism in the Godthaab-Fiskenaesset region, southern West Greenland. Journal of Metamorphic Geology **8**, 171-190.

Rickwood 1968: Detailed Instructions for Recalculation of Garnet Analyses into End-Member Molecules by the Proposed Scheme.

Robert, F. 1996: Quartz-carbonate vein gold. In: Geology of Canadian Mineral Deposit Types. Geology of Canada, **8**, 350-366. Ottawa: Geological Survey of Canada.

Robinson, P.; Spear, F.S.; Schumacher, J.C.; Laird, J.; Klein, C.; Evans, B.W. and Doolan, B.L. 1982: Amphiboles: Petrology and Experimental Phase Relations. In: Reviews in Mineralogy, 159-182.

Schneiderman, J.S. and Tracy, R.J. 1991: Petrology of orthoamphibole-cordierite gneisses from the Orijärvi area, southwest Finland. American Mineralogist **76**, 942-955.

Simmons, S.F.; White, N.C. and John, D.A. 2005: Geological characteristics of Epithermal Precious and Base Metal Deposits. Economic Geology, One Hundredth Anniversary Volume **1905-2005**, 485-522.

Spear, F.S. 1993: Metamorphism of ultramafic and cordierite-anthophyllite rocks. In: Metamorphic Phase Equilibria and Pressure-Temperature-Time Paths, Chapter **13**, 469-489.

Taylor, S.R.; Capp, A.C. and Graham, A.L. 1969. Trace Element Abundances in Andesites II. Saipan, Bougainville and Fiji. Controls on Mineralogy and Petrology **23**, 1-26.

Taylor, S.R.; Kaye, M.; White, A.J.R.; Duncan, A.R. and Ewart, A. 1969b: Genetic significance of Co, Cr, Ni, Sc and V content of andesites. Geochimica et Cosmochimica Acta **33**, 275-286.

The mineral Pentlandite. Retrieved 13 May 2007 from http://www.galleries.com/minerals/sulfides/pentland/pentland.htm

Yardley, B.W. 1989: Metamorphism of basic igneous rocks. An Introduction to Metamorphic Petrology, 91-125.